IEEE Access
Multidisciplinary | Rapid Review | Open Access Journal

IEEE POWER & ENERGY SOCIETY SECTION

Received 12 April 2023, accepted 28 April 2023, date of publication 3 May 2023, date of current version 10 May 2023.

Digital Object Identifier 10.1109/ACCESS.2023.3272836

RESEARCH ARTICLE

Load Frequency Control Using Golden Eagle Optimization for Multi-Area Power System Connected Through AC/HVDC Transmission and Supported With Hybrid Energy Storage Devices

IRFAN AHMED KHAN[1], HAZLIE MOKHLIS[1,2], (Senior Member, IEEE), NURULAFIQAH NADZIRAH MANSOR[1], (Senior Member, IEEE), HAZLEE AZIL ILLIAS[1], (Senior Member, IEEE), MUHAMMAD USAMA[1,3], AMIL DARAZ[4], LI WANG[4,5], (Senior Member, IEEE), AND LILIK JAMILATUL AWALIN[2]

[1]Department of Electrical Engineering, Faculty of Engineering, Universiti Malaya, Kuala Lumpur 50603, Malaysia
[2]Faculty of Advanced Technology and Multidiscipline, Universitas Airlangga, Gedung Kuliah Bersama UNAIR Kampus C, Surabaya 60155, Indonesia
[3]Department of Electrical Engineering, Rachna College of Engineering and Technology, Gujranwala 52250, Pakistan (A Constituent College of University of Engineering and Technology, Lahore, Pakistan)
[4]School of Information Science and Engineering, NingboTech University, Ningbo 315100, China
[5]Department of Electrical Engineering, National Cheng Kung University, Tainan 70101, Taiwan

Corresponding authors: Hazlie Mokhlis (hazli@um.edu.my) and Lilik Jamilatul Awalin (lilik.j.a@ftmm.unair.ac.id)

This work was supported in part by the Universiti Malaya through the International Collaboration under Grant ST027-2022, and in part by the Impact-Oriented Interdisciplinary Research under Grant IIRG001A-2020IISS.

ABSTRACT The reliability of a power system depends on its ability to handle fluctuations and varying load demands, as uncontrolled frequency deviations can lead to load-shedding and blackouts. Optimally tuned controllers are essential for Load Frequency Control (LFC) applications to efficiently stabilize the power system by minimizing frequency undershoots, overshoots, and settling time. This paper proposed the application of novel Golden Eagle Optimization (GEO) algorithm for the optimal tuning of the LFC controller, which has not been previously employed in any LFC applications. Moreover, this paper presents the first-ever implementation of a hybrid energy storage system consisting of Vanadium Redox Flow Battery (VRFB) and Super Magnetic Energy Storage System (SMES) coupled with AC/HVDC transmission lines in a multi-area power system. A GEO optimized Proportional-Integrative-Derivative (GEO-PID) robust controller is designed with the Integral Time Absolute Error (ITAE) objective function to enhance the power system's stability. The proposed controller is tested on two and four areas power systems considering the sensitivity and nonlinearity of the power systems. A robustness test is also performed to verify the stability of the system under randomly chosen loading conditions. In comparison with particle swarm optimization, dragonfly algorithm, sine cosine algorithm, ant lion optimization, and whale optimization algorithm, the GEO-PID controller significantly reduced the settling time up to 80% for different area's frequencies. Simulation results indicate that the proposed controller outperforms other recent optimization algorithms by effectively dampening the frequency and tie-line deviations with less settling times, as well as reduced frequency undershoots and overshoots.

INDEX TERMS Energy storage system, golden eagle optimization, load frequency control, super magnetic energy storage system (SMES), vanadium redox flow battery.

I. INTRODUCTION

A power system reliability relies on its ability to handle disturbances, fluctuations, and varying load demands.

The associate editor coordinating the review of this manuscript and approving it for publication was Elizete Maria Lourenco.

An unstable power system can cause load-shedding, and in the most severe cases, a total blackout of the system may occur. Varying load demands cause the system frequency and power flows in the tie-line to fluctuate from their nominal values [1], [2]. Power systems are typically linked with several power-generating areas in order to supply power to regions that are in need of high levels of power. As power systems are interconnected, disruptions in one area may affect other areas. Thus, the stability of the system's frequency becomes one of the primary concerns of the system operators [3], [4]. Load Frequency Control (LFC) is the process of maintaining frequency within the nominal limits under changes in load demand [5]. Power system stability relies heavily on LFC to ensure power balance between interconnected areas under varying load conditions [6], [7]. The frequency of the system will become imbalanced if the load demand of the system exceeds or falls behind the generator's power. An automated control action initiates the necessary action to maintain the nominal frequency, either by starting load shedding or by triggering protection relays to disconnect generators [8].

For LFC applications, optimally tuned controllers play a vital role to stabilize the power system efficiently by minimizing frequency undershoots, overshoots, and settling time. Due to their simplicity and efficiency, Optimized Proportional-Integrative-Derivative (PID) controllers remain popular and widely used in industry. In spite of this, from the literature, it appears that many researchers have been working on the design of modern controllers which are often derived from PID, fractional order, fuzzy, or artificial neural networks. From the literature review, a two-area system is controlled by a hybrid proportional–fractional order integral–derivative and fuzzy proportional–integral–derivative ($PI^{\lambda}D$-$FPI^{\lambda}D$) controller fine-tuned with a symbiotic organism search algorithm [9]. A fuzzy-based proportional derivation with filter (FPDF) and proportional–integral (PI) cascaded controller (FPDF+PI) with sunflower optimization is investigated to enhance system stability under loading conditions [10]. The salp swarm algorithm (SSA) has been applied to optimize a fuzzy PID with a filter controller for multi-area LFC applications [11]. Using the whale optimization technique, a fuzzy tilt integral derivative (FTID) with a filter plus double integral (FTIDF-II) controller has effectively damped frequency oscillations [12]. Under variable loading conditions, a FOPI-PDF (Fractional order proportional integral-proportional derivative with filter) controller for frequency stabilization of diverse hybrid power systems is proposed [13]. A fuzzy-PD-PI controller is developed and executed in a three-area power system using Grasshopper Optimization Algorithm (GOA) optimization tweaked with Integral Time Absolute Error (ITAE) cost function [14]. In a microgrid with an ITAE objective function, the imperialist competitive algorithm (ICA) is employed to optimize the cascaded PDF and one plus PI (C-PDF(1 + PI)) controller, where the proposed controller efficiently damp frequency oscillations with less settling time [15].

The recent development in LFC studies focused on designing new controllers, employing the latest optimization techniques, and integrating hybrid energy storage systems. A parallel fuzzy-based fractional order Proportional-Integrative (PI) and PID with filter (FFOPI + PIDN) controller is tuned using a quasi-opposition-based equilibrium optimization (QOEO) algorithm for a multi-area power system and its settling time response is found better than the PID controller [16]. A Proportional-Derivative (PD) with filter cascaded PI (PDn-PI) controller is used with the coyote optimization method which results in better settling time than the PI and PID controllers [17]. A PID controller is employed with an Artificial Rabbits Optimization Algorithm in an isolated microgrid with hybrid energy sources for effective system stability [18]. The Manta Ray Foraging Optimization (MRFO) approach has been introduced for configuring the PID controller's gain settings in control loops of a system. It considers non-linearities like GRC and GDB and includes PV and wind power plants, along with plug-in electric vehicles, flywheels, and capacitive energy storage systems [19]. In a two-area hybrid power system, an improved MRFO algorithm is employed, to tune a cascaded hybrid fractional order and tilt integrator differentiator with filter (FOTPID-TIDF) which has three degrees of freedom. The proposed LFC method enhances power system stability and performance by effectively reducing uncertainty and renewable generation variations, with fast convergence and minimal objective function values [20].

Controllers employed with metaheuristic algorithms can stabilize the variations to a certain extent but to achieve further stability in a power system, Energy Storage Systems (ESSs) are essential. The implementation of ESSs contributes to LFC by providing virtual inertia into the power system in the event of sudden load demand. ESS devices such as Super Magnetic Energy Storage System (SMES) and Vanadium Redox Flow Battery (VRFB) have emerged as virtual inertia sources in the power system. They provide frequency regulation by injecting or absorbing power from or into the grid, ensuring dynamic frequency control. Among other energy storage devices, SMES have a high efficiency of 95% with a fast-dynamic response of less than 100ms and a life cycle of 20+ years making it ideal for LFC regulation. While VRFBs have an efficiency of 85% with a storage backup of 2 to 10 hours and can respond within milliseconds [21]. SMES can be charged and discharged rapidly without adversely affecting its lifespan, while VRFBs have a long lifespan because of their separated electrolyte design that eliminates contamination risks and their ability to be fully discharged, which prevents capacity degradation over time unlike lithium batteries [22]. VRFBs and SMESs have attained great attention from researchers for LFC in multi-area power systems. In a two-area power system, VRFB application coupled with a thyristor-controlled phase shifter is presented for robust control of load variations [23]. In a two-area power system, VRFB integrated

with Thyristor Controlled Series Compensator (TCSC) outperformed the LFC exhibiting less overshoot, undershoot, and settling time [24]. In [25], SMES and TCSC devices are incorporated to improve the system stability of a two-area power system. A three-area thermal power system, equipped with VRFB is investigated for dynamic frequency regulation [26]. A Fractional Oder Proportional Integrative Derivative (FOPID) controller-based disturbance rejection scheme is proposed for a three-area hybrid power system based on VRFB to provide virtual inertia to damp frequency fluctuations effectively [27]. In [28], SMES is proposed with a hybrid fractional order PID and tilt integral derivative (FOPID-TID) controller to provide virtual inertia for damping the electromechanical oscillations.

In power systems, the interconnection of multi-area power systems is not only linked through AC tie-lines but some systems are also connected through HVDC tie-lines. HVDC transmission lines facilitate bulk power transfer over long distances with fewer losses. Furthermore, it helps connecting multi-area power systems of different frequencies. From the literature, a multi-area power system interconnected with AC and HVDC parallel tie-lines is investigated for LFC application [29], [30]. In a three-area system, HVDC and ESS are proposed with an Artificial Neural Network (ANN) based PID-GOA controller for LFC [31]. HVDC tie-line and SSSC devices are incorporated in a two-area power system to enhance LFC stability [32].

PID controllers are simple and efficient, making them a popular choice for LFC problems. However, artificially intelligent and modern controllers involve complex computation and requires an elevated level of expertise. Additionally, fuzzy logic controllers have implementation challenges due to the assumptions made for assigning membership functions, while ANN controllers need lots of data and retraining if the model changes. Although these controllers seem superior to PID but they are not commonly used in industry. Also, various meta-heuristic approach algorithms have the disadvantages of trapping at local minima, premature convergence, and complex computation. It is important to note that most of the literature did not address the application of their proposed approaches to the large multi-area power system and also without considering the Generation Rate Constraint (GRC) and Governor Deadband (GDB) nonlinearities. Moreover, limited studies were conducted using parallel AC-DC tie-lines on a multi-area power system. Hybridization of VRFB and SMES, combining the advantages of high-capacity and high-performance energy storage systems, can lead to providing a robust response under various loading conditions. The novelty aspect of this work is further verified through the Web of Science (WoS) database [33] and found that the hybrid implementation of VRFB and SMES with AC/HVDC link has never been investigated in the past.

The major contributions of the present work are highlighted as follows:

1. To design and implement, for the first time, a GEO-PID controller using Golden Eagle Optimization for LFC applications.
2. To implement a hybrid energy storage system that consists of VRFB and SMES, coupled with AC/HVDC parallel tie-lines.
3. To analyze GRC and GDB non-linearities on a large multi-area power system.
4. To perform a sensitivity analysis of the proposed controller by changing the system parameters and explore the robustness under variable load disturbances.

The organization of this paper is as follows: Section II presents the LFC model in a multi-area power system with HVDC, SMES, and VRFB followed by an overview of the GEO algorithm and designing of a GEO-PID controller is presented. The simulation results and discussion are presented in Section III. Section IV presents the conclusion.

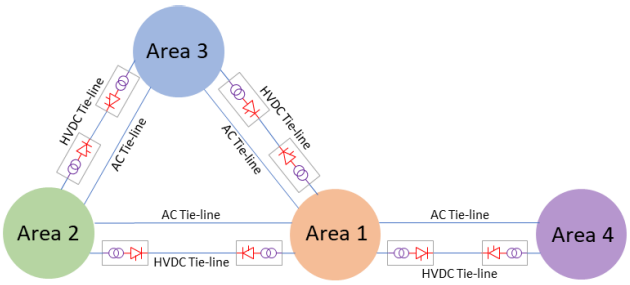

FIGURE 1. Generalized model of a four-area power system.

II. INTERCONNECTED POWER SYSTEM MODEL

A. LFC MODEL

An interconnected four-area power system model based on LFC is illustrated in Fig. 1 and Fig. 2. The system in Fig. 1 consists of parallel AC and HVDC tie-lines, which are interconnected among the four areas for the bidirectional flow of power. The addition of HVDC tie-lines reduces the load on AC transmission lines and increases power transfer abilities between two power system areas. A detailed four-area thermal power system based on transfer functions is designed for Matlab/Simulink environment as illustrated in Fig. 2. This model is commonly used for analyzing four-area power systems [34], [35], [36], [37]. With a nominal load of 1000MW, each area has a power rating of 2000MW. PID controllers are installed in each area along with the turbine, generator, speed governing system, and load. The transfer functions of the governor, turbine, and power system are indicated in (1)-(3).

$$G_G(s) = \frac{K_g}{1 + sT_g} \tag{1}$$

$$G_T(s) = \frac{K_t}{1 + sT_t} \tag{2}$$

$$G_P(s) = \frac{K_p}{1 + sT_p} \tag{3}$$

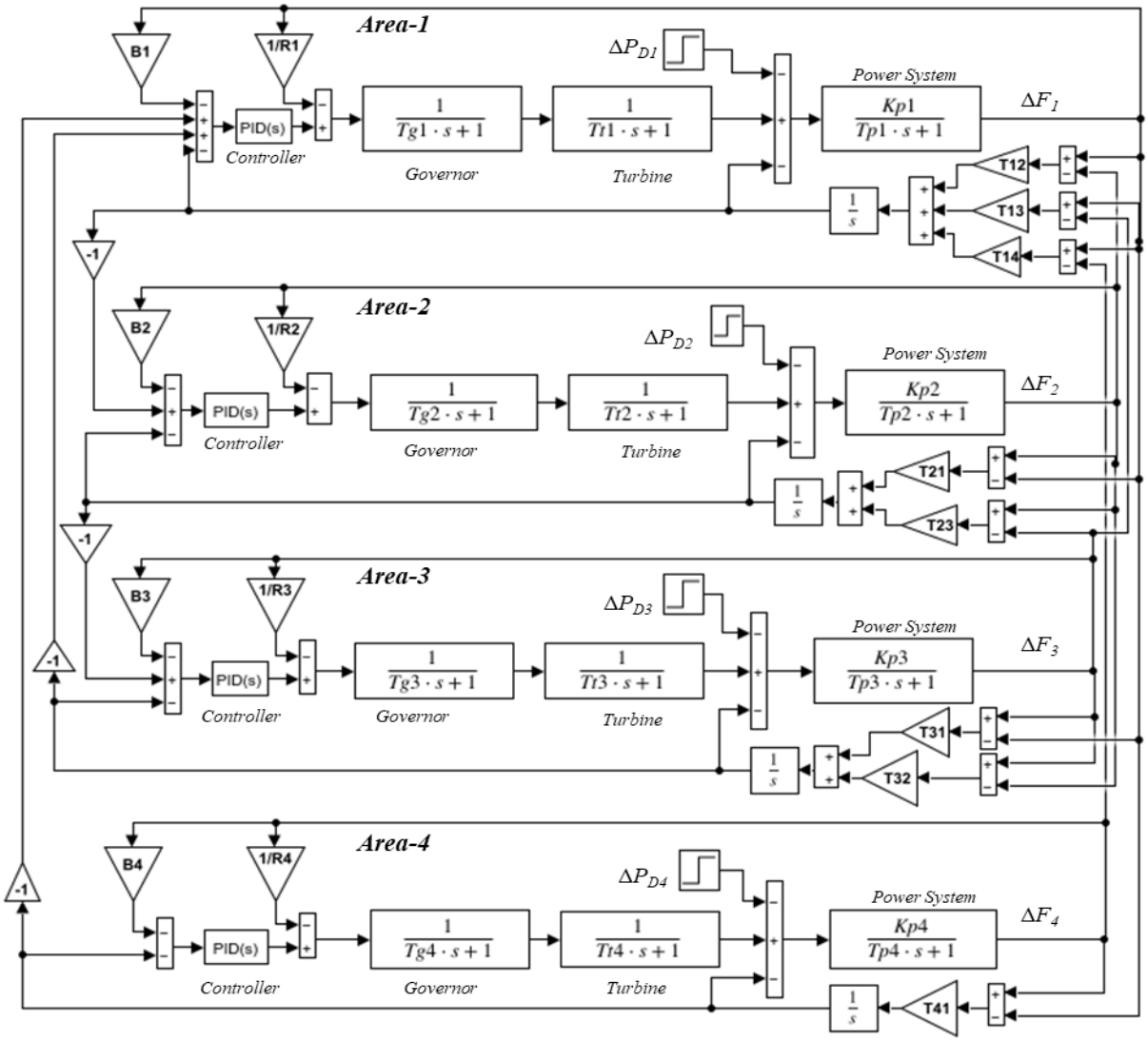

FIGURE 2. LFC of a four-area power system model.

For each area, K_g, K_t, and K_p are the gains of speed governor, turbine, and power system, respectively. The time constant of the speed governor, turbine, and power system is represented as T_g, T_t, and T_p respectively. ΔP_D is the change in load demand, ΔP_{tie} is the change in tie line power, ΔF is the system frequency deviation, and T_{21}, T_{12}, T_{13}, T_{31}, T_{23}, T_{32}, T_{14}, and T_{41} are the tie-line synchronizing coefficients. *ACE* represents the area control error which is also an input to the controller, B is the frequency bias parameter, *and* R is the parameter for governor speed regulation.

B. LINEARIZED HVDC MODEL

In this paper, parallel AC and HVDC transmission lines are examined for the bidirectional flow of power between interconnected areas. Equation (4) illustrates a linearized model of an HVDC link where ΔF represents the frequency deviation in ith area, K_{DC} denotes the gain of the HVDC link and T_{DC} is the time it takes for DC current to settle after a step load perturbation [2], [38]:

$$\Delta P_{tie,DC} = \frac{K_{DC}}{1 + sT_{DC}} \Delta F \tag{4}$$

C. GOVERNOR DEADBAND

Governor Deadband (GDB) refers to "the magnitude of a sustained speed change where the valve position of the turbine does not change" [39]. The governor of a large thermal generator takes some time to respond to a change in valve position when the load and power generation are mismatched until the input signal reaches a threshold value. Thus, such non-linearities must be considered in thermal power plant modeling. The transfer function model of GDB is illustrated in (5) [40]. GDB is typically 0.06%, as allowed by the joint AIEE-ASME standards (American Institute of

Electrical Engineers and American Society of Mechanical Engineers) [41], [42], [43]. This value provides sufficient sensitivity while maintaining stability and reliability. The GDB nonlinearity tends to produce a continuous sinusoidal oscillation with a natural period of about two seconds. Therefore, a backlash of 0.05% is chosen for the simulation [44].

$$G_{GDB}(s) = \frac{0.8 - s(0.2/\pi)}{1 + sT_g} \tag{5}$$

D. GENERATION RATE CONSTANT

Physical constraints should be considered when analyzing the realistic AGC system. Generation Rate Constant (GRC) is the critical physical constraint for the rate of change of generating power, primarily because of mechanical and thermal stress on both the governor and turbine [30]. The GRC Simulink model is presented in Fig. 3.

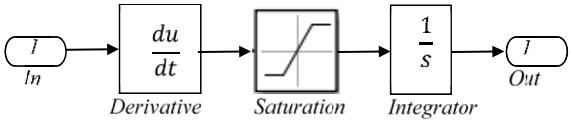

FIGURE 3. GRC model.

E. SUPER MAGNETIC ENERGY STORAGE DEVICE

The SMES provide frequency regulation by injecting or absorbing power from or into the grid to maintain the system frequency. The SMES transfer function model is illustrated in Fig. 4, which is established with a two-stage lead-lag compensator [2], [30]. Where P_{SMES} is the generated output power, T_1, T_2, T_3, and T_4 are the time constants of a lead-lag block, and K_{SMES} and T_{SMES} are the gain and time constant of the SMES, respectively.

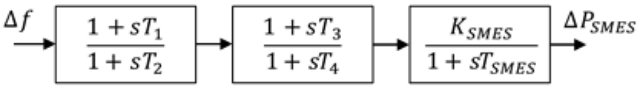

FIGURE 4. SMES model.

F. VANADIUM REDOX FLOW BATTERY

Vanadium redox flow battery also referred to as RFB in this study, is known to be excellent energy storage devices as well as being capable of responding rapidly ensuring dynamic frequency control. The VRFB transfer function model for LFC is presented in Fig. 5. Where K_{RFB} is the gain of VRFB, T_{dRFB} is the time delay constant, K_{rRFB} and T_{cRFB} are the gain and time constant to reset VRFB. The VRFB has been designed with the restriction that the maximum permissible discharge of energy must equal the maximum permissible deposit of energy. As a result, the limit of P_{Min} and P_{Max} have been set equal to -0.01 and 0.01 p.u. respectively [45].

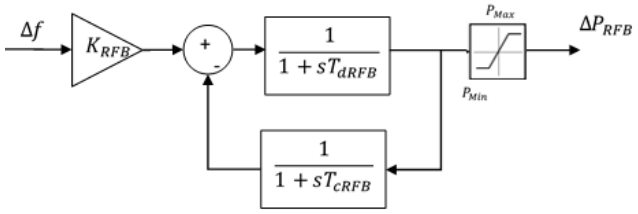

FIGURE 5. VRFB model.

TABLE 1. GEO parameters setting.

Parameter Settings	Values	Parameter Settings	Values
Maximum iterations	200	Initial attack propensity	0.5
Population size	50	Final Attack propensity	2
Lower bound	0	Initial cruise propensity	1
Upper bound	15	Final cruise propensity	0.5

TABLE 2. Optimized controller gains for a two-area power system.

	Area 1			Area 2		
	K_P	K_I	K_D	K_P	K_I	K_D
PSO	2.125	4.958	0.421	2.066	4.595	0.628
SCA	2.168	5.002	0.534	5.001	4.820	1.543
DA	2.393	5.103	0.677	4.987	4.901	1.339
WOA	0.877	3.755	0.321	2.042	5.047	0.476
ALO	2.401	4.960	0.667	2.918	4.971	0.828
GEO	1.874	5.472	0.539	2.568	5.998	0.677

G. GOLDEN EAGLE OPTIMIZATION FOR MULTI-AREA POWER SYSTEM

Golden Eagle Optimization (GEO) solves the global optimization problem using a nature-inspired swarm-based metaheuristic algorithm. Golden eagles usually cruise and hunt in a spiral trajectory as shown in Fig. 6, so the prey stays to one side of them. In addition, they survey other regions in order to find better food. Each golden eagle begins its hunt by flying in large circles within its realm at high altitudes. After spotting prey, it moves around the perimeter of a hypothetical circle centered around the prey. Golden eagles memorize prey's location but continue to circle it. Gradually lowering their altitude, eagles circle their prey closer and closer, downsizing the radius around it. While doing so, it also searches the surrounding areas for better prey. The location of a golden eagle's best prey is shared with other eagles. When it cannot find better prey, it keeps circling around until it attacks the prey. Upon discovering a new prey, the eagle will forget about the old one and fly around the new one. To find the best prey, an eagle balances attack and cruise

TABLE 3. Comparison of settling time, overshoot, undershoot, and objective functions with various optimization algorithms for case 1.

		ALO	DA	PSO	SCA	WOA	GEO
Settling time (s)	ΔF_1	4.254	6.21	3.437	5.558	4.267	1.88
	ΔF_2	4.206	5.299	2.727	3.071	4.170	2.025
	$\Delta Ptie_{12}$	4.487	6.732	4.143	6.708	4.379	3.644
Overshoot (p.u.)	ΔF_1	0.0004511	0.0006822	0.0012601	0.0010827	0.0007465	0.0004865
	ΔF_2	-	0.0000402	0.0000516	-	0.0000459	0.0000389
	$\Delta Ptie_{12}$	0.0000362	0.0001058	0.0002052	0.0001412	0.0000248	0.0000202
Undershoot Overshoot (p.u.)	ΔF_1	-0.0037312	-0.0037056	-0.0044994	-0.0040942	-0.0052887	-0.0041240
	ΔF_2	-0.0029837	-0.0023308	-0.0034384	-0.0022219	-0.0038616	-0.0032742
	$\Delta Ptie_{12}$	-0.0001631	-0.0004411	-0.0002776	-0.0006951	-0.0005698	-0.0002101
Objective Function	IAE	0.004197	0.004338	0.005426	0.004758	0.005441	0.003998
	ISE	1.672e-5	1.44e-5	2.671e-5	1.742e-5	3.866e-5	2.036e-5
	ITSE	2.953e-6	3.068e-6	4.858e-6	3.712e-6	6.237e-6	3.015e-6
	ITAE	0.001601	0.002532	0.002102	0.002789	0.001524	0.001142

propensities simultaneously. A mathematical model has been developed in [46] to describe global optimization's exploration and exploitation properties. The golden eagle attacks its prey which is mathematically modeled using a vector that begins at its current location and finishes at its prey location. Equation (6) represents the attack vector as follows:

$$\vec{A}_i = \vec{X}_f^* - \vec{X}_i \tag{6}$$

where $\vec{A}_i = [a_1, a_2, \ldots, a_n]$ represents the attack vector of an ith golden eagle, $X_i = [x_1, x_2, \ldots, x_n]$ represents the decision/design variables vector, and $X_f^* = [x_1^*, x_2^*, \ldots x_n^*]$ represents the best location of prey found by golden eagle f. As this algorithm guides the best-visited locations to the golden eagles, it is classified as an exploitation phase.

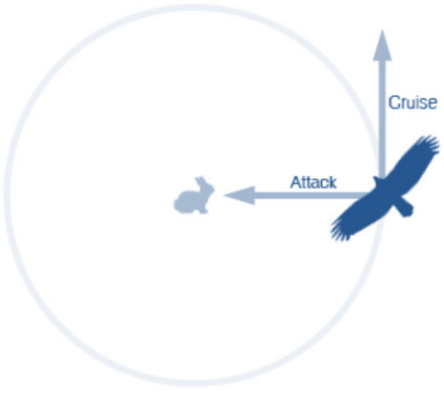

FIGURE 6. A golden eagle's trajectory [46].

Golden eagles explore their search space by using cruise vectors to find better prey. This vector is perpendicular to the attack vector, and it is the tangential vector of the circle. A cruise vector with n-dimensions is located on a circle's tangent hyperplane. The first step is to determine the tangent hyperplane equation. An n-dimensional hyperplane is

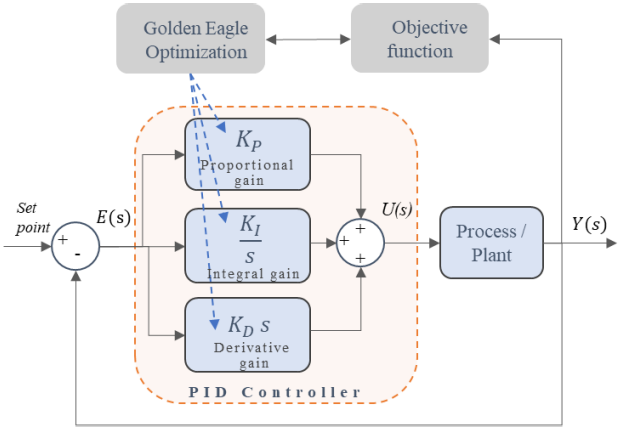

FIGURE 7. Block diagram of GEO-PID controller.

expressed as a scalar expression in (7). Using (8), we can determine the hyperplane on which the cruise vector (9) lies.

$$d = \sum_{j=1}^{n} h_j x_j \tag{7}$$

$$\sum_{j=1}^{n} a_j x_j = \sum_{j=1}^{n} a_j^t x_j^* \tag{8}$$

$$\vec{C}_i = (c_1, c_2, \ldots, c_k, \ldots, c_n) \tag{9}$$

where $\vec{H} = [h_1, h_2, \ldots, h_n]$ represents the normal vector, a_j represents the element of j^{th} attack vector, and t represents the current iteration number. A cruise vector randomly selects one variable from $n-1$ variables as a fixed variable, but one whose attack vector element is non-zero, and assigns random values to the remaining n free vectors. By using (10) the value of the fixed variable can be identified.

$$c_k = \frac{d - \sum_{j,j\neq k} a_j}{a_k} \tag{10}$$

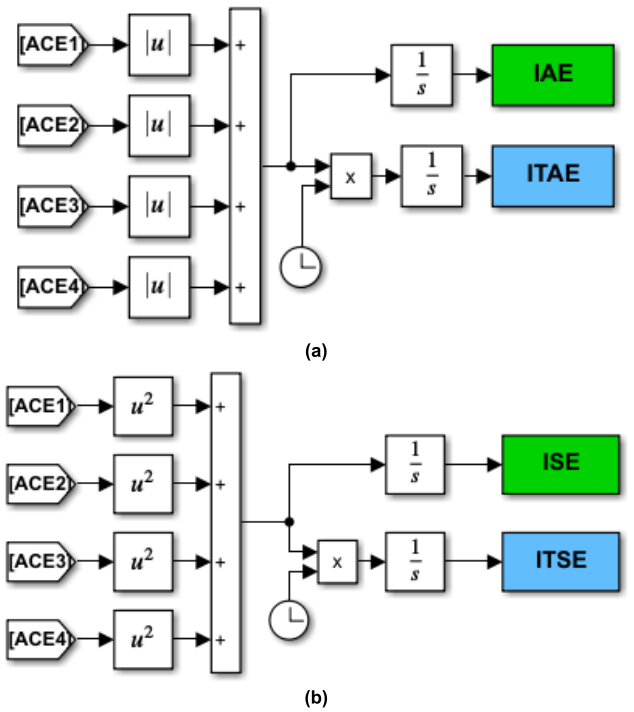

FIGURE 8. Objective function modeling in Simulink (a) for IAE and ITAE (b) for ISE and ITSE.

where k represents the fixed variable index, c_k represents the kth element of the cruise vector (exploitation), and a_k represents elements of the kth attack vector. Attack and cruise constitute the golden eagle's displacement. The golden eagle's new position is determined by (11) and its step vector is shown in (12).

$$x^{t+1} = x^t + \Delta x_i^t \tag{11}$$

$$\Delta x_i = \vec{r}_1 p_a \frac{\vec{A}_i}{\|\vec{A}_i\|} + \vec{r}_2 p_c \frac{\vec{C}_i}{\|\vec{C}_i\|} \tag{12}$$

where, $\|\vec{A}_i\| = \sqrt{\sum_{j=1}^{n} a_j^2}$ and $\|\vec{C}_i\| = \sqrt{\sum_{j=1}^{n} c_j^2}$ are Euclidean norms, $\vec{r}_1$ and $\vec{r}_2$ are random vectors and have elements bounded by interval [0,1].

$$p_c = p_c^0 - \frac{t}{T}\left|p_c^T - p_c^0\right| \tag{13}$$

$$p_a = p_a^0 + \frac{t}{T}\left|p_a^T - p_a^0\right| \tag{14}$$

Equations (13) and (14) represent coefficients of attack and cruise, p_a and p_c, employed by GEO to transform exploration to exploitation. A low p_a and a high p_c are initially considered. Progressing through iterations, p_a steadily increases while p_c slowly decreases. Where T represents maximum iterations while t denotes the current iteration. p_c^0 and p_c^T represent cruise propensity at initial and final points, and p_a^0 and p_a^T represents the propensity to attack initial and final points. The pseudo-code of GEO is presented in ALGORITHM 1.

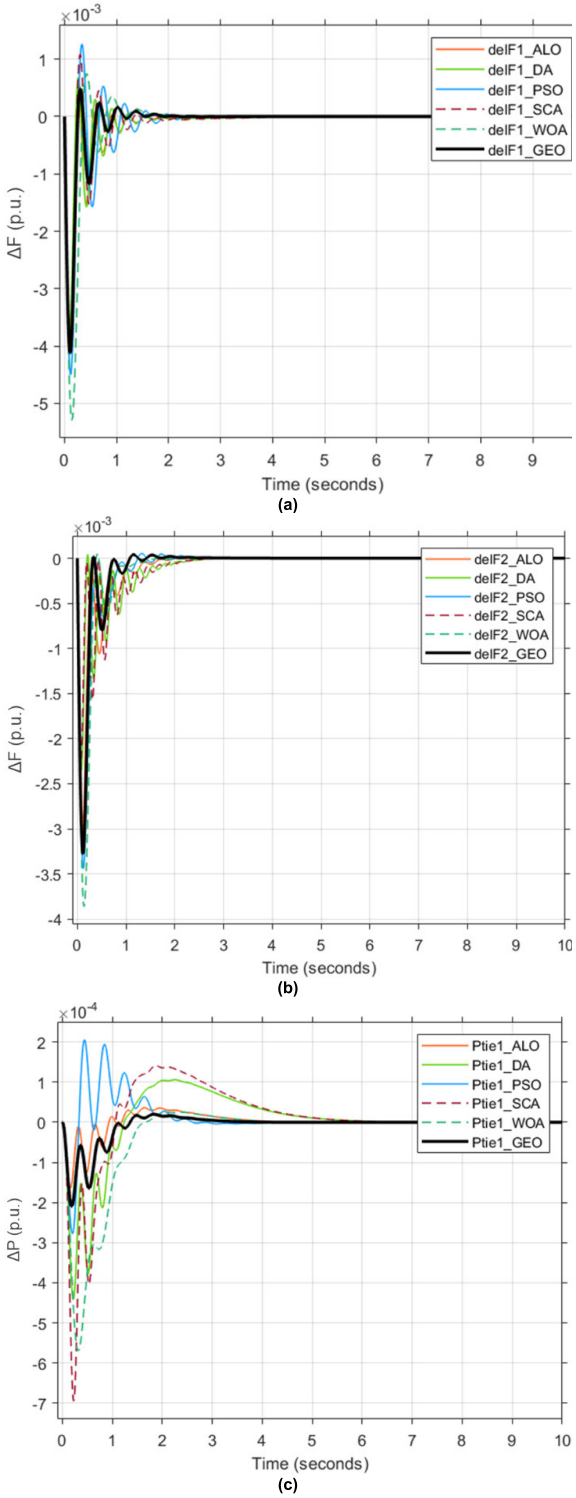

FIGURE 9. Two-area power system with 1% SLP in both areas (a) ΔF_1 (b) ΔF_2 (c) ΔP_{tie12}.

H. DESIGNING OF A GEO-PID CONTROLLER

PID controllers are the most popular single input and single output controllers used in industries because of their simplicity, robustness, and ease of tuning since it has few parameters

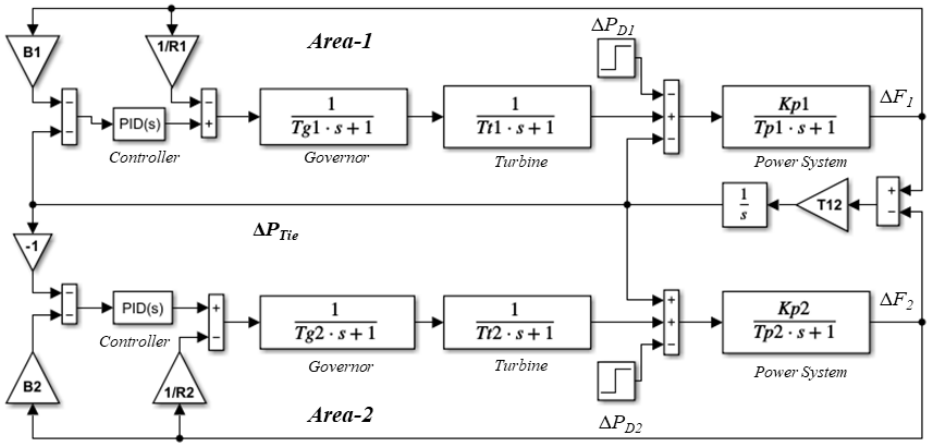

FIGURE 10. Block diagram of a two-area interconnected thermal power system.

Algorithm 1 GEO Pseudo-Code

```
Set the number of variables, population size n, and the number of
iterations T.
Calculate the fitness function
Initialize the population's memory
Initialize p_a and p_c
for each iteration t
    Update p_a and p_c from (13) and (14)
    for every golden eagle i = 1: n
        Pick a random prey based on the population's memory
        If the length of A ≠0 in (6)
            Calculate C and Δx from (9) and (12)
            Update the new position x^{t+1} in (11)
            Analyze the fitness function of the new position x^{t+1}
            If the fitness of the new position x^{C1} is better
            than the one in eagle i's memory
                Update the memory of eagle i
            end if
        end if
    end for
end for
```

to optimize [40], [47], [48]. Controller plays a crucial role in frequency control, which is an essential method used in power systems to maintain a balance between power generation and demand. It maintains the power balance between the generators in each control area to keep the frequency at its set point, such as 50Hz or 60Hz, by adjusting the power output of the generators. The response time for such control usually ranges from 30 seconds to a few minutes [49]. Our proposed controller reduces the response time to less than 10 seconds, resulting in substantial stability.

Furthermore, the PID controller is optimized using GEO methodology that ensures exploration and exploitation phases are balanced, preventing the optimization process from becoming stuck at a local optimal. In addition, GEO is simple to construct and implement, and it is not sensitive to control system parameters. These characteristics allow the proposed approach to be applied to a wide range of complex and multidimensional problems. Furthermore, the results in [46] indicate that GEO belongs to the middle tier of algorithms with respect to computation time, and it can retain its relative computing time against other well-known algorithms in the literature, namely, Particle Swarm Optimization, Genetic Algorithm, Grey Wolf Optimizer, Crow Search Algorithm, Harmony Search, and Dragonfly Algorithm. Thus, GEO's computational time performance is comparable to other algorithms in terms of its efficiency.

To achieve optimum performance of the PID controller, the GEO algorithm is employed with the ITAE, ITSE, IAE, and ISE objective functions to compute the optimum controller gains as illustrated in Fig. 7. The PID controller output transfer function representation is given in (15) where $U(s)$ and $E(s)$ are the control and error signals; K_P, K_I, and K_D are the proportional, integral, and derivative gains of the PID controller, respectively [50].

$$U(s) = \left(K_P + \frac{K_I}{s} + K_D s\right) \cdot E(s) \tag{15}$$

The limits of the controller gains are mentioned in (16) where larger limits require more iterations, resulting in longer computing times. The objective functions are modeled in Simulink as illustrated in Fig. 8. The minimization of J for the GEO-PID controller is subject to:

$$\begin{aligned} K_{P,min} \le K_P \le K_{P,max} \\ K_{I,min} \le K_I \le K_{I,max} \\ K_{D,min} \le K_D \le K_{D,max} \end{aligned} \tag{16}$$

The primary function of the controller is to minimize the difference (error) between the output of the plant and the setpoint. By using the error signal, the objective function together with the optimization algorithm fine-tunes the controller parameter. The objective functions ITAE, ITSE, ISE, and IAE are calculated from (17)-(20) where t is the simulation time and n is the number of areas, ACE is dependent on the frequency and tie-line power deviations [40].

$$J_{ITAE} = \int_0^t t \cdot \sum_{i=1}^{n} |ACE_n| dt \tag{17}$$

TABLE 4. Optimum controller gains for a four-area power system.

	Area 1			Area 2			Area 3			Area 4		
	K_P	K_I	K_D	K_P	K_I	K_D	K_P	K_I	K_D	K_P	K_I	K_D
PSO	10.031	8.599	4.096	8.885	9.765	1.505	8.046	9.566	7.320	9.601	9.395	2.027
SCA	4.149	7.543	2.040	7.204	4.259	1.583	7.559	8.019	8.159	8.696	5.632	4.341
DA	6.328	10.019	1.338	9.997	10.021	2.690	10.001	9.978	2.302	9.987	10.003	2.662
WOA	9.986	9.986	3.025	9.986	9.986	2.814	9.986	9.986	2.769	6.440	9.986	1.563
ALO	7.534	9.989	2.178	9.991	9.505	4.0386	8.091	9.801	1.602	8.492	9.730	2.780
GEO	9.209	14.983	1.863	9.8492	14.957	2.001	9.209	14.607	1.809	8.660	13.741	1.987

TABLE 5. Comparison of settling time, overshoot, and undershoot with various optimization algorithms for case 2.

		ALO	DA	PSO	SCA	WOA	GEO
Settling time (s)	ΔF_1	2.90	5.27	9.23	11.02	4.68	2.17
	ΔF_2	3.13	5.10	8.47	12.70	5.31	2.72
	ΔF_3	3.56	5.57	8.39	9.99	5.98	2.54
	ΔF_4	3.04	4.24	7.36	8.19	6.38	2.49
	$\Delta Ptie_1$	3.25	4.85	8.79	13.37	4.48	2.41
	$\Delta Ptie_2$	2.96	4.44	9.01	10.83	4.07	2.43
	$\Delta Ptie_3$	5.59	4.86	8.97	10.39	5.65	2.28
	$\Delta Ptie_4$	3.18	5.15	9.51	11.40	5.76	2.27
Overshoot ((p.u.)	ΔF_1	-	0.0005097	0.0002875	0.0000573	-	0.0002005
	ΔF_2	-	-	0.0016163	0.0004666	-	0.0002619
	ΔF_3	0.0000316	-	0.0000899	-	-	0.0001950
	ΔF_4	-	-	0.0011909	-	0.0012024	0.0006974
	$\Delta Ptie_1$	0.0004240	0.0003432	0.0004257	0.0004506	0.0006484	0.0002994
	$\Delta Ptie_2$	0.0004214	0.0004595	0.0006002	0.0008313	0.0001016	0.0001548
	$\Delta Ptie_3$	0.0001978	0.0001137	0.0007087	0.0006833	0.0002929	0.0002236
	$\Delta Ptie_4$	0.0000469	0.0002489	0.0001523	0.0003143	0.0000717	0.0000271
Undershoot (p.u.)	ΔF_1	-0.0049862	-0.0062279	-0.0041122	-0.0053496	-0.0042393	-0.0052491
	ΔF_2	-0.0033870	-0.0041080	-0.0052020	-0.0051621	-0.0040467	-0.0047158
	ΔF_3	-0.0060210	-0.0050729	-0.0029620	-0.0037213	-0.0046626	-0.0056434
	ΔF_4	-0.0057777	-0.0058292	-0.0065086	-0.0047299	-0.0074847	-0.0066354
	$\Delta Ptie_1$	-0.0001278	-0.0006999	-0.0005414	-0.0011542	-0.0001581	-0.0001782
	$\Delta Ptie_2$	-0.0002336	-0.0002337	-0.0006513	-0.0003935	-0.0003176	-0.0002656
	$\Delta Ptie_3$	-0.0005122	-0.0004216	-0.0004356	-0.0004678	-0.0000944	-0.0001430
	$\Delta Ptie_4$	-0.0001031	-0.0000922	-0.00030279	-0.0001169	-0.0004583	-0.0001264
Objective Function	IAE	0.004132	0.004003	0.00485	0.00769	0.004085	0.002829
	ISE	4.354e-6	4.588e-6	4.436e-6	6.612e-6	4.56e-6	4.106e-6
	ITSE	1.299e-5	1.238e-6	1.844e-6	4.118e-6	1.292e-6	7.735e-7
	ITAE	0.002455	0.002381	0.004744	0.01103	0.00248	0.0008875

$$J_{ITSE} = \int_0^t t \cdot \sum_{i=1}^{n} (ACE_n)^2 dt \tag{18}$$

$$J_{ISE} = \int_0^t \sum_{i=1}^{n} (ACE_n)^2 dt \tag{19}$$

$$J_{IAE} = \int_0^t \sum_{i=1}^{n} |ACE_n| dt \tag{20}$$

III. SIMULATION RESULTS

In this study, MATLAB/Simulink 2021b environment is used with ode23 solver and variable step to design transfer function models of the studied power systems. The GEO algorithm is implemented and computations related to the objective functions are carried out within the m.file. The optimization process was simulated 20 times with 200 iterations to determine the best optimal gains for the controller.

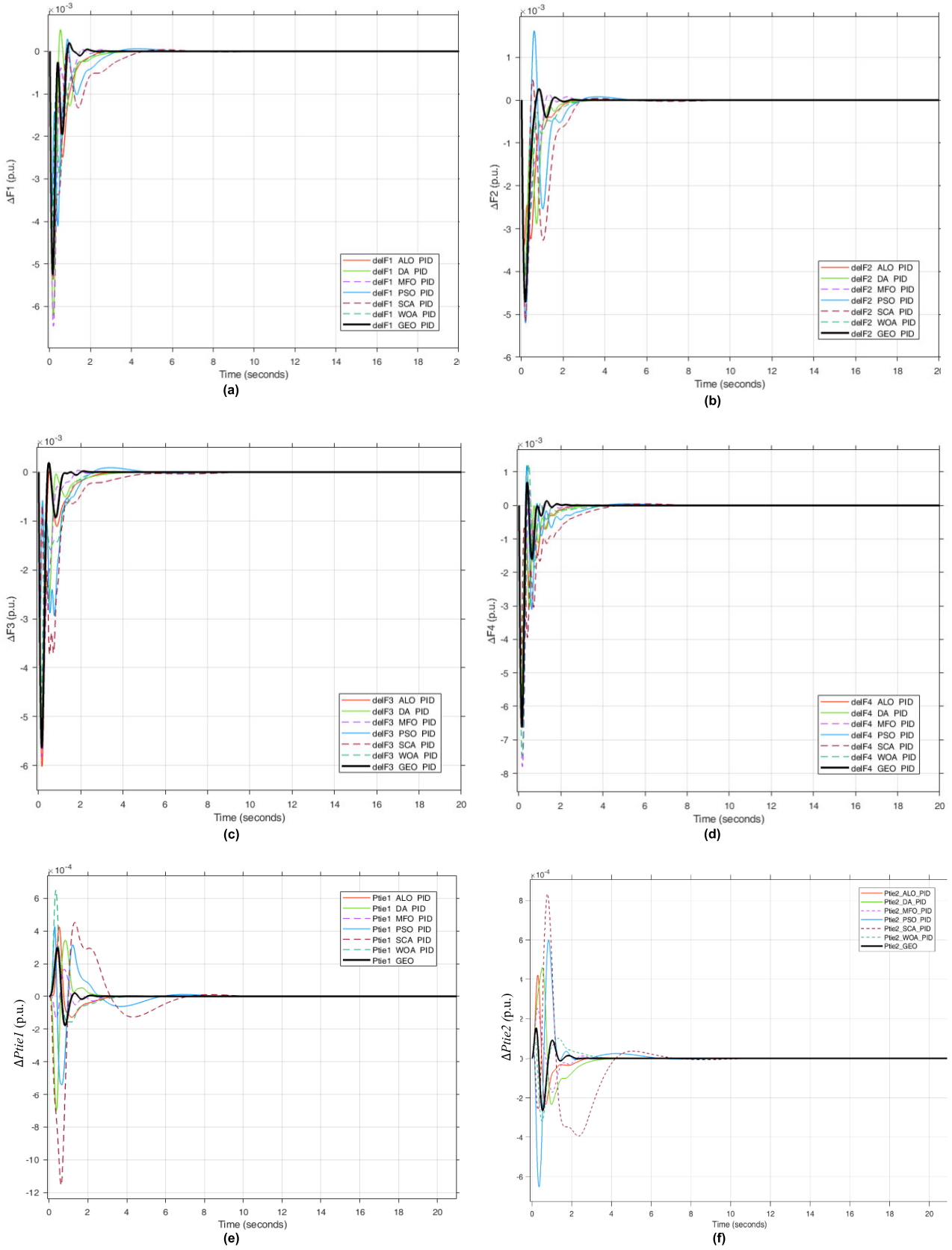

FIGURE 11. Four-area power system with 1% SLP in all areas (a) ΔF_1 (b) ΔF_2 (c) ΔF_3 (d) ΔF_4 (e) ΔP_{tie1} (f) ΔP_{tie2}.

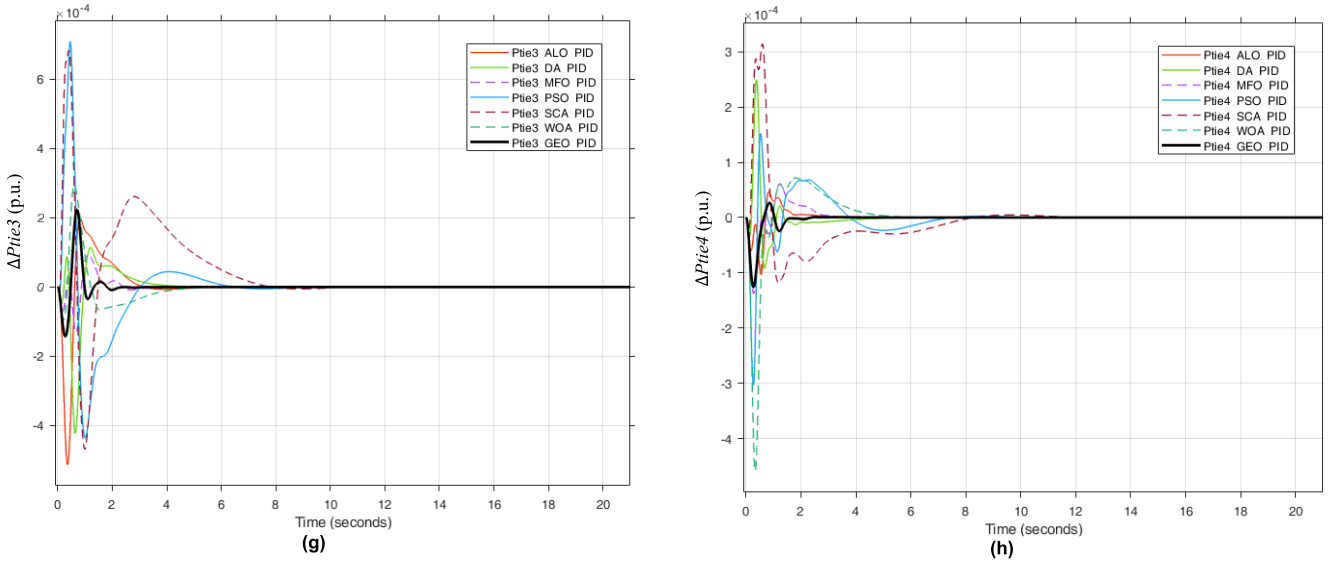

FIGURE 11. *(Continued.)* **Four-area power system with 1% SLP in all areas (g) ΔP_{tie3} (h) ΔP_{tie4}.**

TABLE 6. Comparison of settling time, overshoot, and undershoot of four-area power system with HVDC and SMES.

		AC tie-line	AC-DC tie-lines	SMES with AC-DC tie-lines
Settling time (s)	ΔF_1	2.176	3.793	4.396
	ΔF_2	2.727	3.236	3.766
	ΔF_3	2.536	3.150	2.725
	ΔF_4	2.493	2.787	2.336
	$\Delta Ptie_1$	2.410	4.361	4.850
	$\Delta Ptie_2$	2.436	3.590	4.950
	$\Delta Ptie_3$	2.286	2.820	4.630
	$\Delta Ptie_4$	2.277	2.868	3.949
Overshoot (p.u.)	ΔF_1	0.0002005	0.0000356	-
	ΔF_2	0.0002619	-	-
	ΔF_3	0.0001950	0.0000926	-
	ΔF_4	0.0006974	0.0007975	-
	$\Delta Ptie_1$	0.0002994	0.0002008	0.0001573
	$\Delta Ptie_2$	0.0001548	0.0001275	0.0000658
	$\Delta Ptie_3$	0.0002236	0.0000886	0.0000983
	$\Delta Ptie_4$	0.0000271	0.0000019	0.0000058
Undershoot (p.u.)	ΔF_1	-0.0052491	-0.0047876	-0.0031664
	ΔF_2	-0.0047158	-0.0042487	-0.0030500
	ΔF_3	-0.0056434	-0.0050870	-0.0033414
	ΔF_4	-0.0066354	-0.0059410	-0.0036080
	$\Delta Ptie_1$	-0.0001782	-0.0000481	-0.0000719
	$\Delta Ptie_2$	-0.0002656	-0.0001664	-0.0001105
	$\Delta Ptie_3$	-0.0001430	-0.0001059	-0.0000708
	$\Delta Ptie_4$	-0.0001264	-0.0000905	-0.0000655
Objective Function	IAE	0.002829	0.002803	0.002751
	ISE	4.106e-6	3.116e-6	2.162e-6
	ITSE	7.735e-7	6.332e-7	5.456e-7
	ITAE	0.0008875	0.001257	0.001333

The parameters of GEO optimization parameters are shown in Table 1.

A. CASE 1: APPLICATION OF 1% SLP ON A TWO-AREA POWER SYSTEM

A two-area non-reheat thermal power system without non-linearities is considered as represented in Fig. 10. Both areas are subjected to a step load perturbation (SLP) of 1% (0.01 p.u.). The optimally tuned GEO-PID controller is compared to some recently reported optimization techniques such as Dragonfly Algorithm (DA) [30], Sine Cosine Algorithm (CSA) [51], Ant Lion optimization (ALO) [52], Whale Optimization Algorithm (WOA) [12], and Particle Swarm Optimization (PSO) [38]. The optimized controller gains for each technique are represented in Table 2. The change in frequency and tie-line power are presented in Fig. 9. The settling time for ΔF_1, ΔF_2, and $\Delta Ptie_{12}$ are 1.88s, 2.025s and 3.644s respectively. The GEO-PID controller outperforms by reducing the settling time of ΔF_1 by 55%, 70%, 45%, 66%, 56%; ΔF_2 by 52%, 52%, 26%, 34%, 51%; and ΔP_{12} by 19%, 46%, 12%, 46%, and 17% in comparison with ALO, DA, PSO, SCA, and WOA optimization respectively. The minimum objective function ITAE is 0.001142, achieved with the proposed GEO-PID controller, which is 29%, 55%, 46%, 59%, and 25% smaller than the ALO, DA, PSO, SCA, and WOA optimization, respectively. From Table 3, it is evident that the ITAE value and settling time associated with GEO-PID are the smallest among the other modern optimization techniques.

B. CASE 2: APPLICATION OF 1% SLP ON A FOUR-AREA POWER SYSTEM

A four-area interconnected non-reheat thermal power system without nonlinearities is considered as represented in Fig. 2. To verify the stability of the system an intense case is considered where all areas are subjected to a step load perturbation (SLP) of 1%. The GEO-PID controller is compared with various recent optimization techniques such as

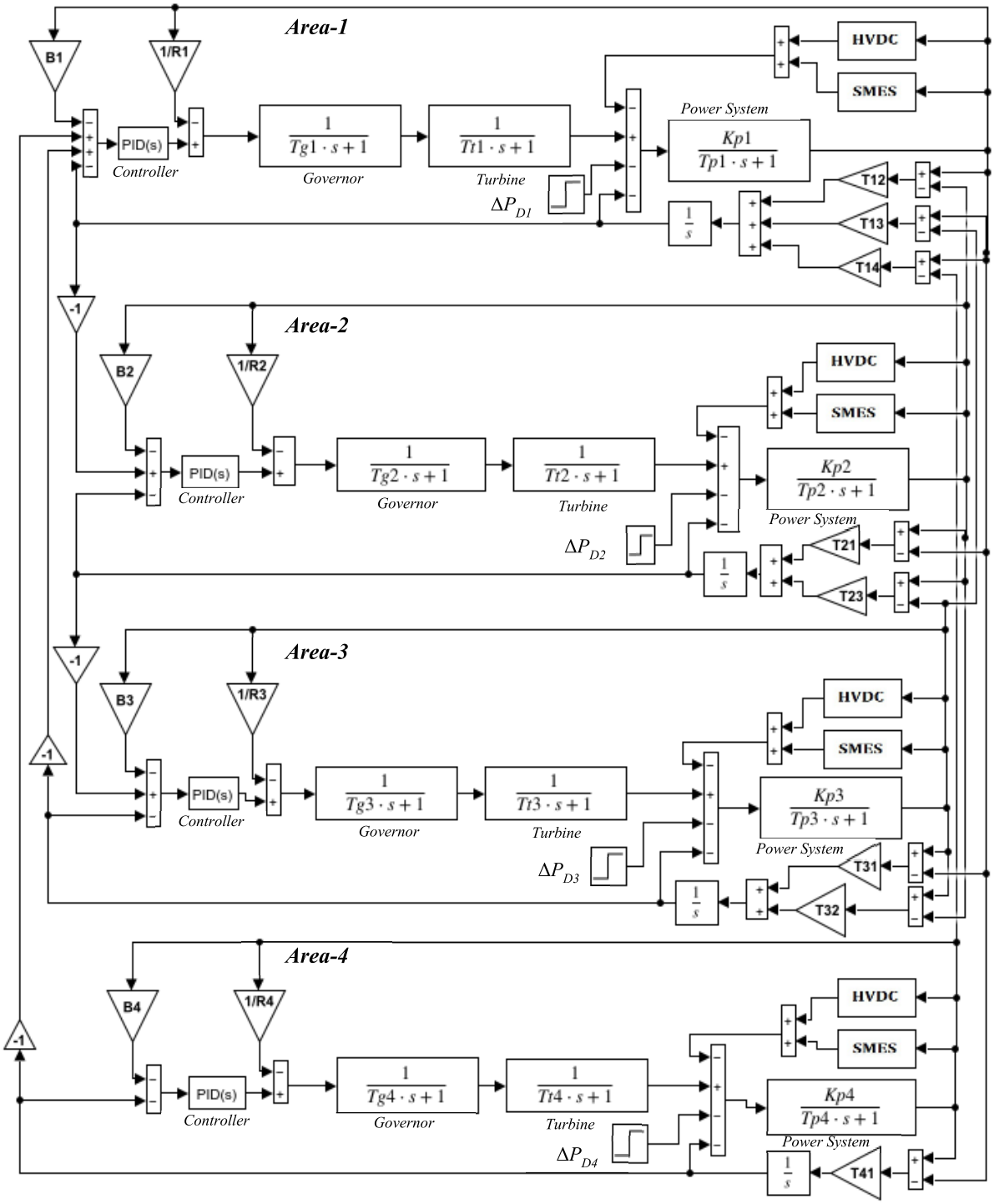

FIGURE 12. Four-area interconnected power system incorporated with SMES and AC-DC tie-lines.

GEO, ALO, DA, PSO, SCA, and WOA algorithms. The optimized controller gains for each technique are represented in Table 4. The change in frequency and tie-line power are shown in Fig. 11. In Fig. 11(b), ΔF_2 obtained from SCA is not changing in an identical manner with other optimization techniques. The reason for this pattern is that the PID controller gain values obtained from SCA optimization for all areas are far deviated when compared with the other optimization techniques as shown in Table 4, where the value of integral gain (K_I) for SCA is 4.259 which is almost half as compared to other optimization algorithms. Another possible reason is that the optimal solution depends on the number of iterations

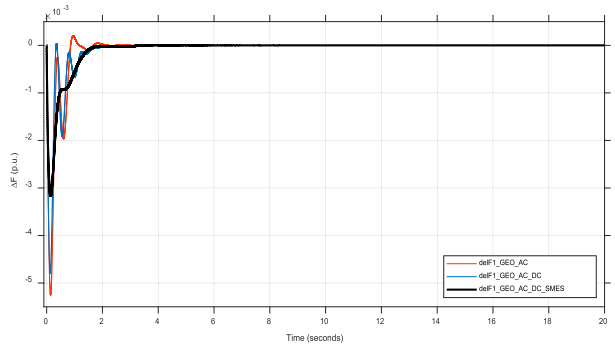

(a)

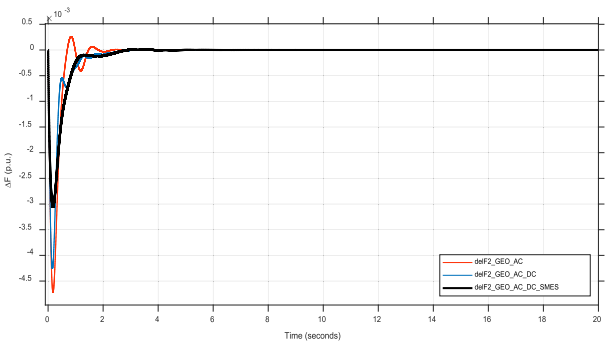

(b)

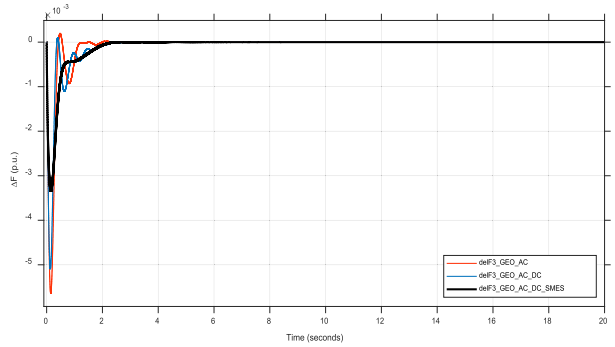

(c)

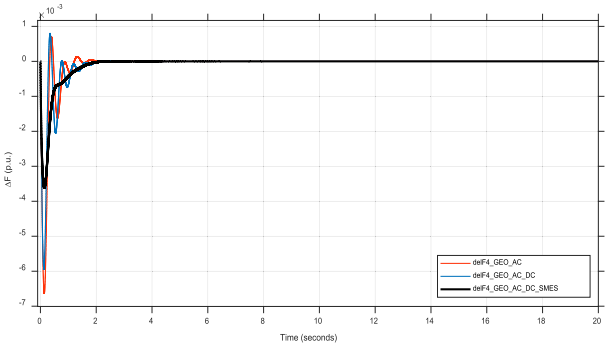

(d)

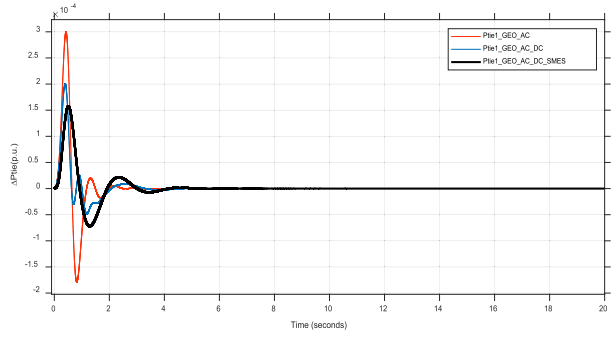

(e)

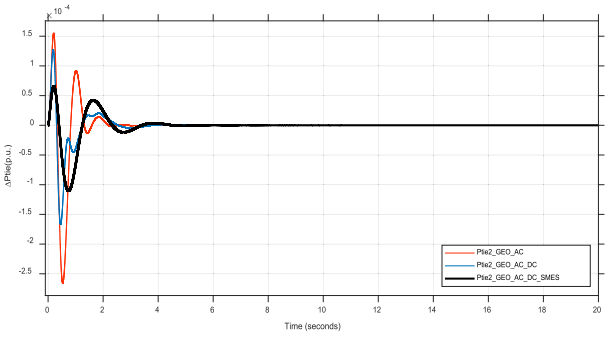

(f)

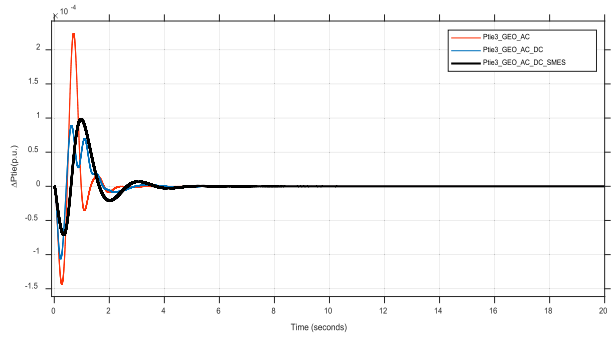

(g)

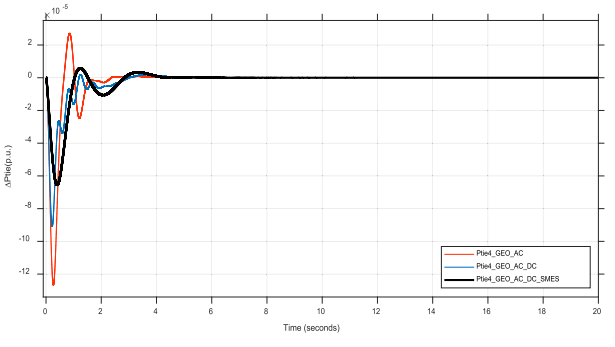

(h)

FIGURE 13. Four-area power system with HVDC and SMES (a) ΔF1 (b) ΔF2 (c) ΔF3 (d) ΔF4 (e) ΔPtie1 (f) ΔPtie2 (g) ΔPtie3 (h) ΔPtie4.

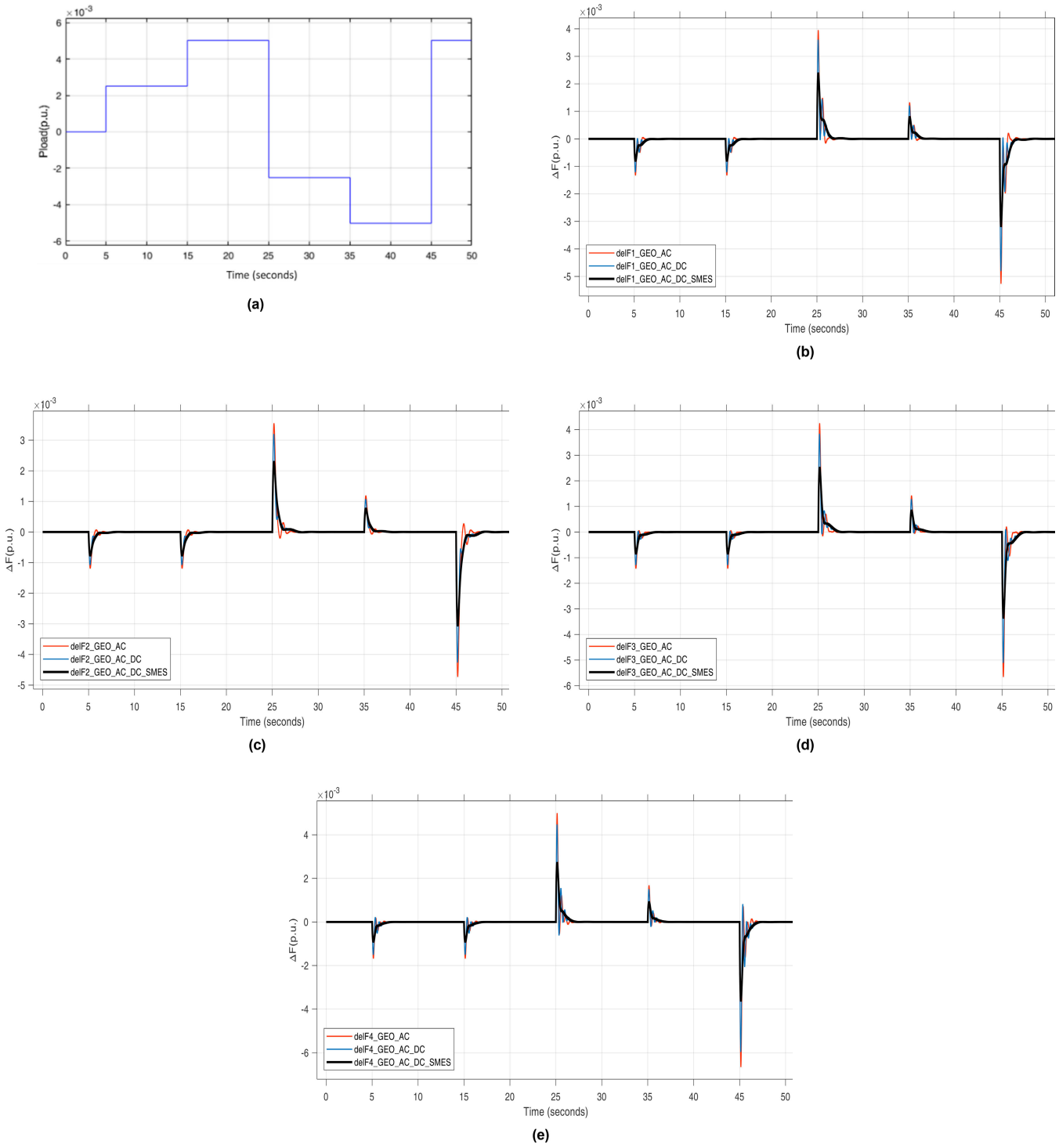

FIGURE 14. Dynamic responses of GEO-PID controller under random load conditions (a) random load (b) ΔF_1 (c) ΔF_2 (d) ΔF_3 (e) ΔF_4.

to find the optimal solution. Some algorithms are able to find the optimal solution in a short number of iterations; however, others require more iterations to reach the optimal solution. The optimized settling time for ΔF_1, ΔF_2, ΔF_3, and ΔF_4 are 2.17s, 2.72s, 2.54s, and 2.49s respectively. While $\Delta Ptie_1$, $\Delta Ptie_2$, $\Delta Ptie_3$, and $\Delta Ptie_4$ are 2.41s, 2.43s, 2.28s, and 2.27s respectively.

The GEO-PID controller outperforms in stabilizing the system by reducing the settling time for ΔF_1 by 25%, 59%, 76%, 80%, 54%; ΔF_2 by 13%, 47%, 68%, 79%, 49%; ΔF_3

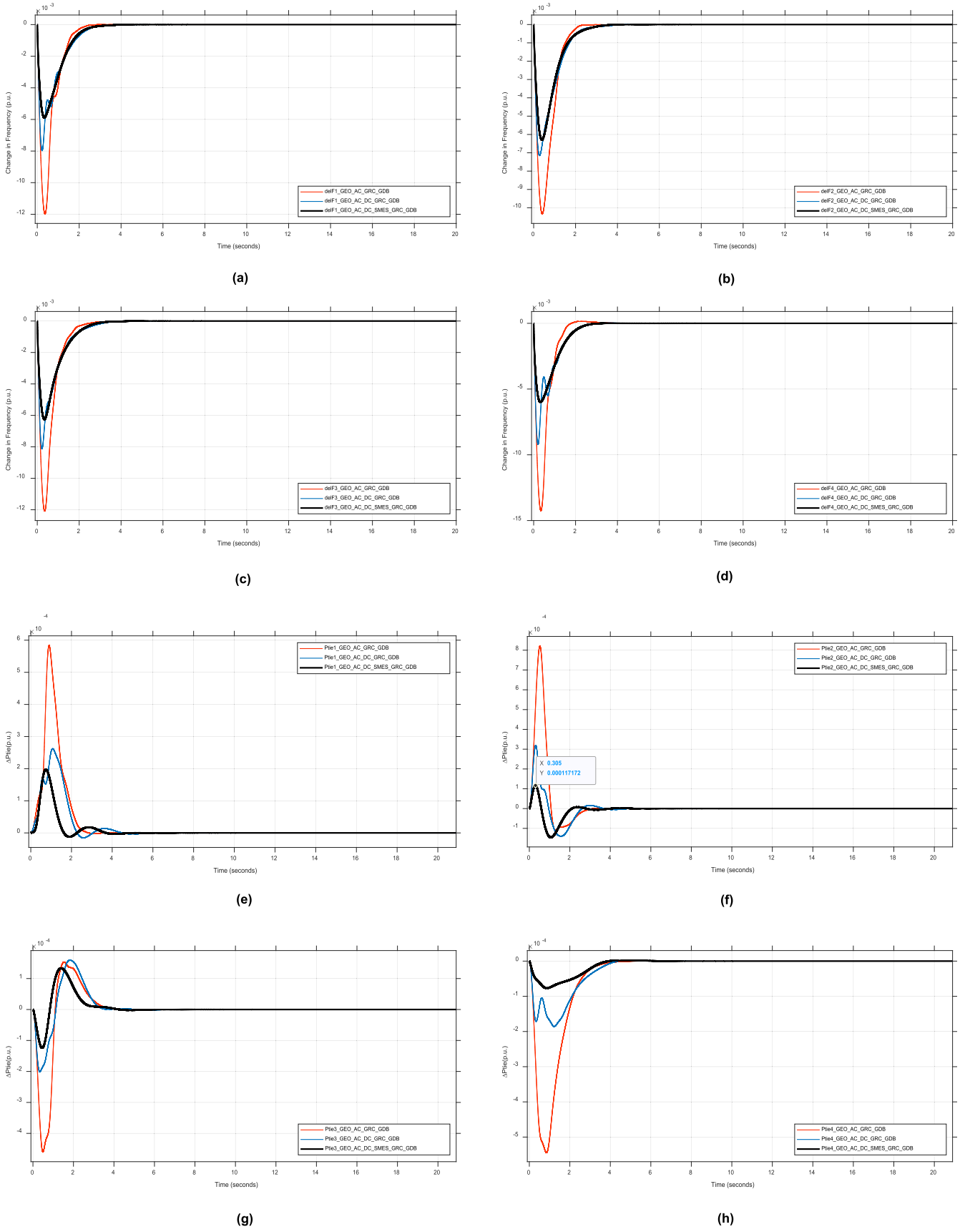

FIGURE 15. Effect of GRC and GDB system non-linearities (a) ΔF_1 (b) ΔF_2 (c) ΔF_3 (d) ΔF_4 (e) ΔP_{tie1} (f) ΔP_{tie2} (g) ΔP_{tie3} (h) ΔP_{tie4}.

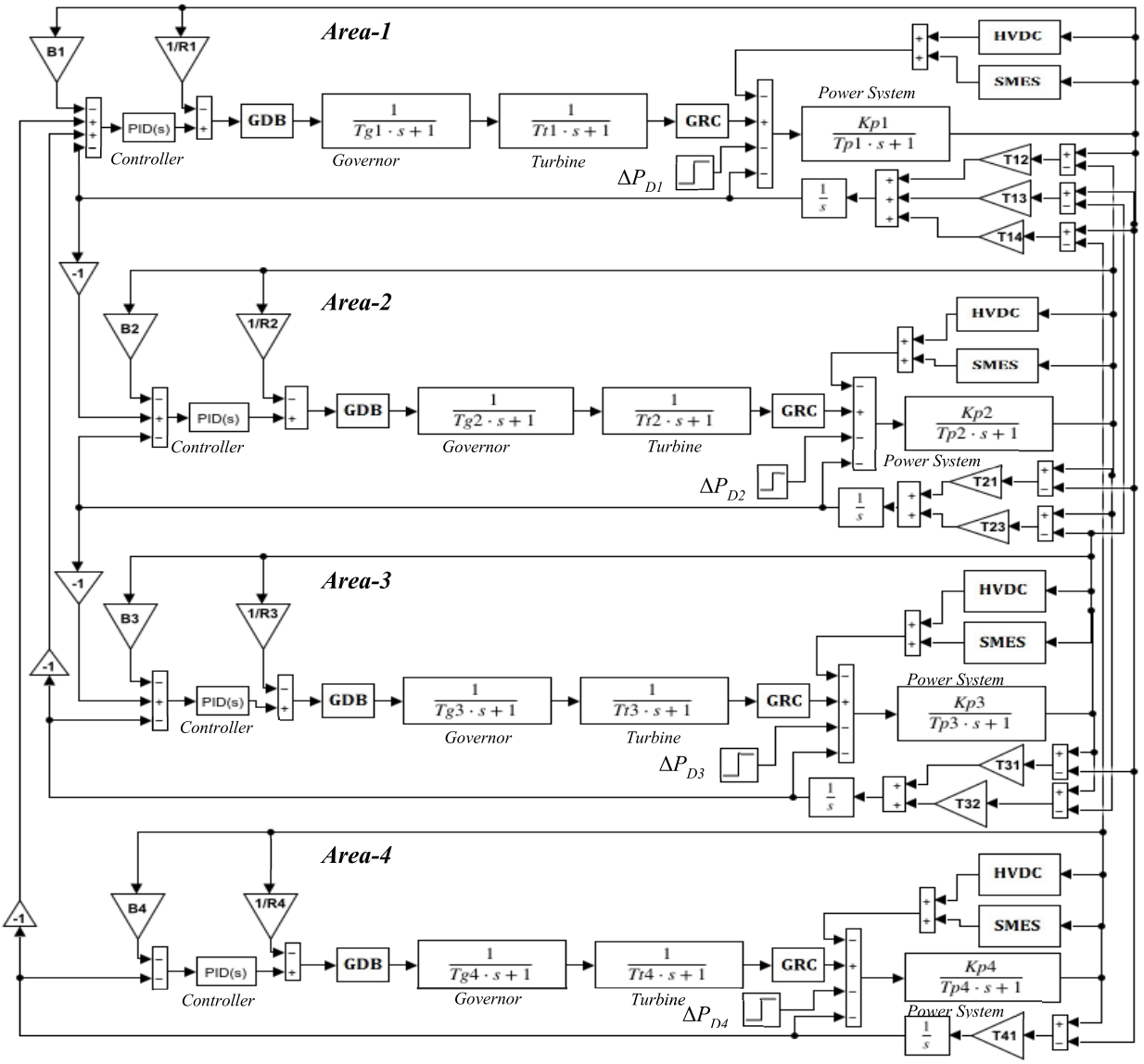

FIGURE 16. Four-area power system incorporated with SMES and AC-DC tie-lines examined with GRC and GDB non-linearities.

by 29%, 54%, 70%, 75%, 58%; F_4 by 18%, 41%, 66%, 70%, 61%; $\Delta Ptie_1$ by26%, 50%, 73%, 82%, 46%; $\Delta Ptie_2$ by 18%, 45%, 73%, 78%, 40%; $\Delta Ptie_3$ by 59%, 53%, 75%, 78%, 60%; and $\Delta Ptie_4$ by 29%, 56%, 76%, 80%, and 61%; in comparison with the ALO, DA, PSO, SCA, and WOA optimization respectively. The minimum objective function ITAE is 0.0008875, achieved with the proposed GEO-PID controller, which is 64%, 63%, 81%, 95%, and 64% smaller than the ALO, DA, PSO, SCA, and WOA optimization, respectively. From Table 5, it is evident that the ITAE value and settling time associated with GEO-PID is the smallest among the other modern optimization techniques.

C. CASE 3: IMPLEMENTATION OF SMES WITH AC-DC PARALLEL TIE-LINES

The effect of SMES coupled with the AC-DC parallel transmission lines is investigated in a four-area power system with 1% SLP applied on all areas as shown in Fig. 12. The optimized GEO-PID controller gains illustrated in Table 4 are used for system stability. The results are compared with a normal AC tie-line, AC-DC link, and hybrid of AC-DC tie-line and SMES. From Fig. 13, the hybrid implementation of AC-DC tie-line and SMES hybrid has substantially reduced frequency undershoots to 40%, 35%, 40%, and 45% for each area, respectively, without any overshoots in comparison with the AC tie-line. Similarly, for each area, the tie-line power undershoots are reduced to 59%, 58%, 50%, and 48%. And tie-line power overshoots are reduced to 47%, 57%, 56%, and 78% respectively with an ITAE value of 0.001333.

The addition of parallel AC-DC link and SMES have an additive advantage over the AC tie-line and AC-DC link respectively for fewer under and overshoots. However, from Table 6, the settling time of the hybrid model is slightly more than the AC and AC-DC link, but it is within a range of

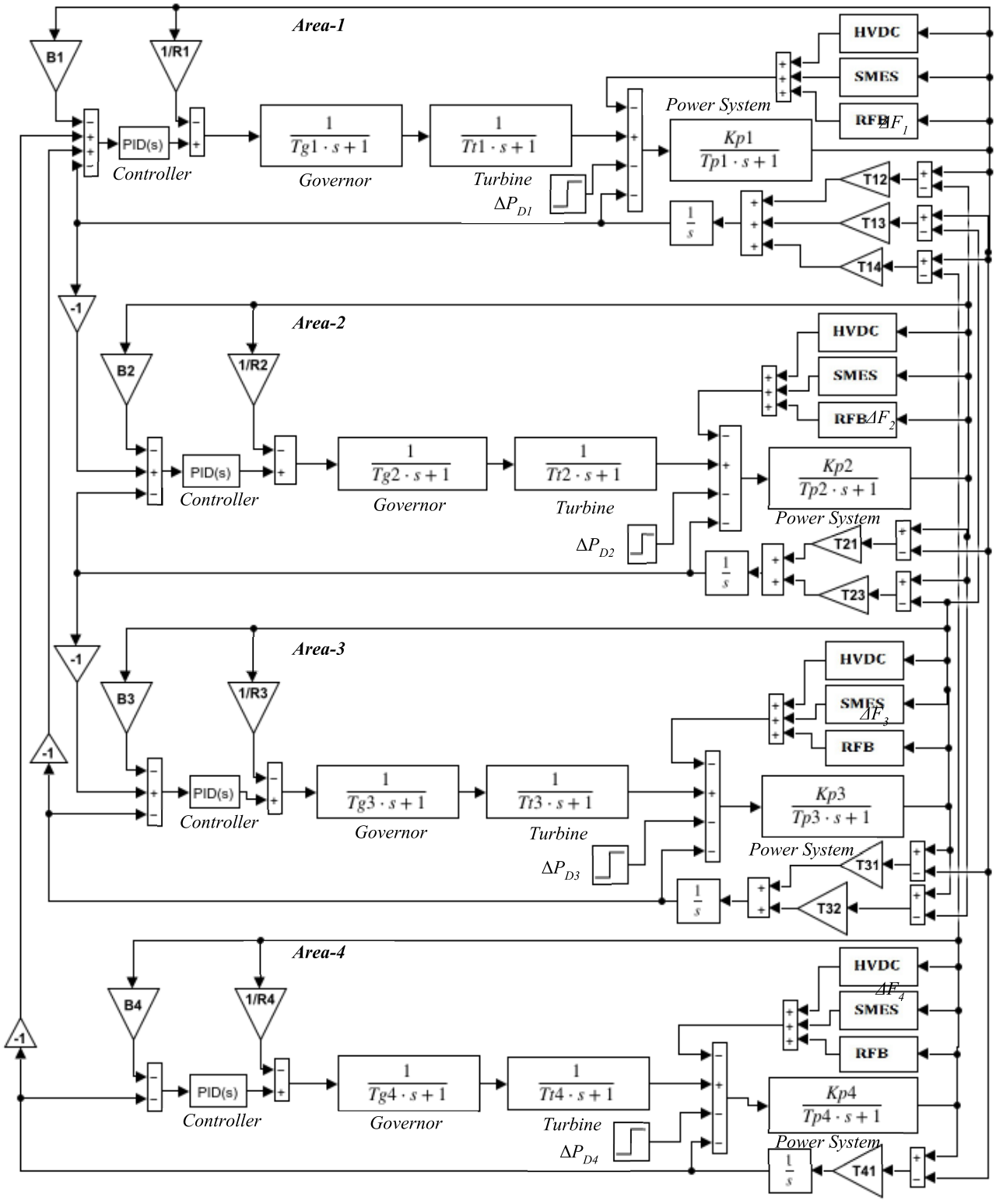

FIGURE 17. LFC of a four-area power system with HVDC tie-line and hybrid virtual inertia injection from SMES and VRFB.

2.336 to 4.95 seconds which is still lesser than the traditional large multiarea power system. From this simulation, it is evident that the hybrid implementation of AC-DC link and SMES is beneficial for the multi-area large power system, where maintaining the under and overshoots are critical under load disturbance. Simulated results indicate that the proposed

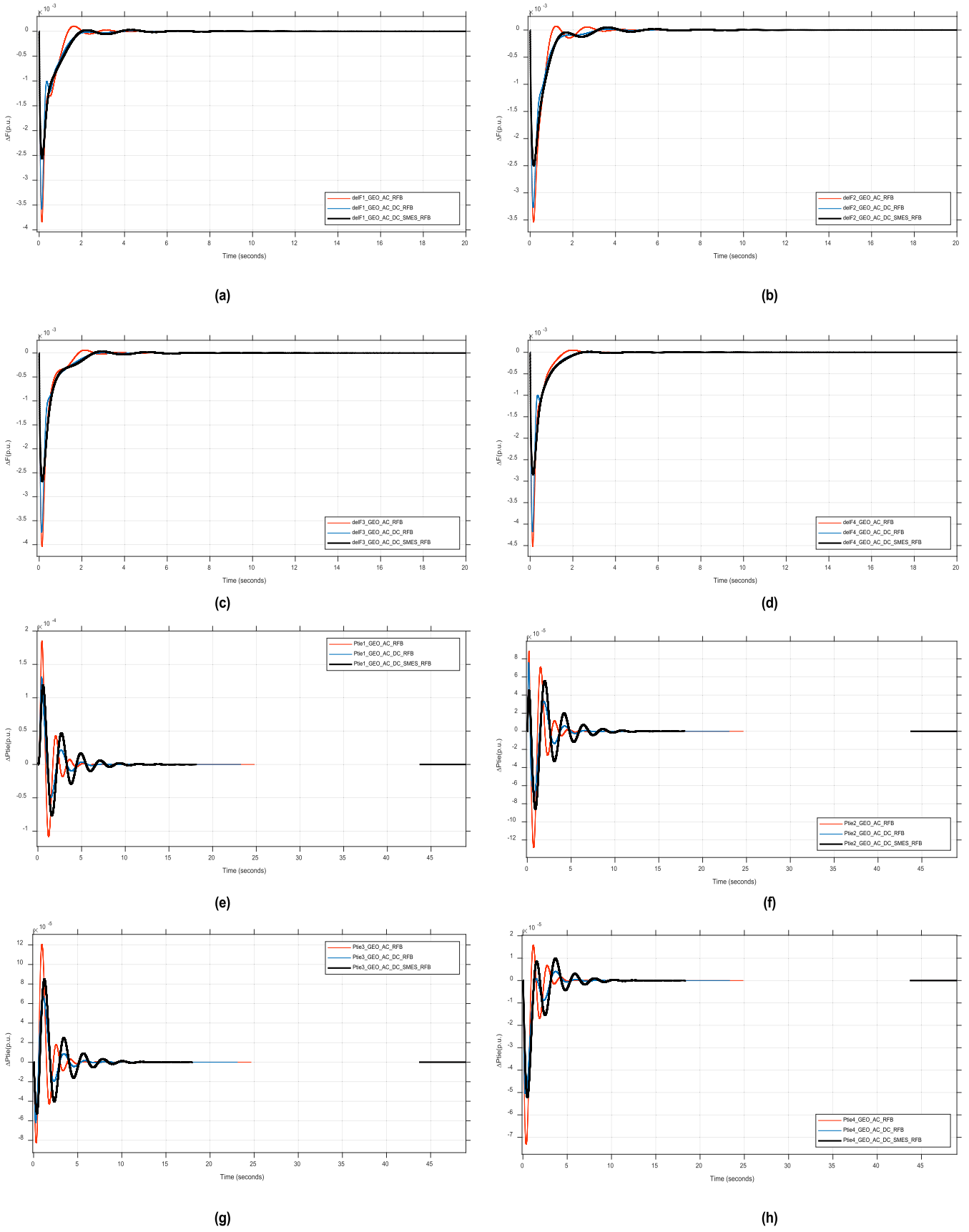

FIGURE 18. LFC through a hybrid implementation of SMES and VRFB (a) ΔF_1 (b) ΔF_2 (c) ΔF_3 (d) ΔF_4 (e) ΔP_{tie1} (f) ΔP_{tie2} (g) ΔP_{tie3} (h) ΔP_{tie4}.

GEO-PID controller works seamlessly with the integration of HVDC and SMES by using the same controller gains of the AC tie line obtained in case 2. From the figures, it is clearly evident that the AC-DC link and hybrid of SMES effectively minimize the deviation peaks and fluctuations of frequency and tie-line power.

TABLE 7. Effect of GRC and GDB system non-linearities on settling time, overshoot, and undershoot.

		AC tie-line	AC-DC tie-lines	SMES with AC-DC tie-lines
Settling time (s)	ΔF_1	2.911	4.995	4.438
	ΔF_2	4.706	4.528	4.271
	ΔF_3	4.730	5.438	4.842
	ΔF_4	5.241	4.740	3.859
	$\Delta Ptie_1$	3.375	5.690	4.711
	$\Delta Ptie_2$	3.919	5.830	4.885
	$\Delta Ptie_3$	4.214	6.319	5.397
	$\Delta Ptie_4$	4.667	5.967	5.594
Overshoot (p.u.)	ΔF_1	-	-	-
	ΔF_2	-	-	-
	ΔF_3	-	-	-
	ΔF_4	0.0001423	-	-
	$\Delta Ptie_1$	0.0005835	0.0002622	0.0001973
	$\Delta Ptie_2$	0.0008212	0.0003198	0.0001171
	$\Delta Ptie_3$	0.0001534	0.0001593	0.0001330
	$\Delta Ptie_4$	-	-	-
Undershoot (p.u.)	ΔF_1	-0.0119804	-0.0079743	-0.005875
	ΔF_2	-0.0103391	-0.0071543	-0.0062932
	ΔF_3	-0.0120817	-0.0081337	-0.0062492
	ΔF_4	-0.0142495	-0.0092118	-0.0059893
	$\Delta Ptie_1$	-	-1.523e-6	-1.2123e-5
	$\Delta Ptie_2$	-0.0001090	-0.0001392	-0.0001454
	$\Delta Ptie_3$	-0.0004604	-0.0002009	-0.0001243
	$\Delta Ptie_4$	-0.0005445	-0.0001857	-7.6862e-5
Objective Function	IAE	0.01449	0.012	0.011
	ISE	5.187e-5	2.361e-5	1.875e-5
	ITSE	2.33e-5	1.186e-5	1.077e-5
	ITAE	0.008825	0.009157	0.008774

D. CASE 4: ROBUSTNESS TEST - RANDOM LOAD APPLICATION

An additional analysis of the proposed controllers is performed by using a random load pattern with SLP in the range of -0.5% to 0.5% applied on all areas of case-3 as represented in Fig. 14(a). The GEO-PID controller's dynamic responses comparison among AC, AC- DC link, and hybrid of AC-DC link and SMES is illustrated in Figs. 14(b)-14(e) for change in frequency and tie-line power. In response to a large load fluctuation at 45s interval, the integration of SMES has significantly suppressed the frequency oscillations by 32%, 28%, 34%, and 39% in all four areas, respectively. Additionally, each area stabilizes within 4.37s, 3.76s, 2.72s, and 2.3s using the proposed methodology. Moreover, the figures clearly illustrate the significant impact of the hybrid installation of AC-DC link and SMES has notably reduced the peaks and fluctuations of frequency and tie-line power. Simulation results confirmed that the GEO-PID controller maintains power system stability across a wide range of load disturbances in a multi-area power system.

TABLE 8. Comparison of settling time, overshoot, and undershoot for hybrid implementation of SMES and VRFB.

		VRFB with AC tie-line	VRFB with AC-DC tie-line	VRFB and SMES with AC-DC tie-line
Settling time (s)	ΔF_1	5.764	4.921	7.054
	ΔF_2	5.388	4.307	7.470
	ΔF_3	5.558	4.710	7.788
	ΔF_4	4.724	4.574	7.541
	$\Delta Ptie_1$	5.382	6.543	10.606
	$\Delta Ptie_2$	4.960	5.902	9.991
	$\Delta Ptie_3$	5.142	6.14	10.212
	$\Delta Ptie_4$	4.485	4.36	8.268
Overshoot (p.u.)	ΔF_1	0.0001052	-	0.0000287
	ΔF_2	0.0000701	-	0.0000485
	ΔF_3	0.0000605	-	0.0000332
	ΔF_4	0.0000516	-	0.0000131
	$\Delta Ptie_1$	0.0001851	0.0001306	0.0001189
	$\Delta Ptie_2$	0.0000885	0.0000756	0.0000557
	$\Delta Ptie_3$	0.0001206	0.0000671	0.0000847
	$\Delta Ptie_4$	0.0000157	0.0000041	0.0000984
Undershoot (p.u.)	ΔF_1	-0.0038380	-0.0035773	-0.0025601
	ΔF_2	-0.0035384	-0.0032657	-0.0024943
	ΔF_3	-0.0040394	-0.0037381	-0.0026764
	ΔF_4	-0.0045226	-0.0041768	-0.0028384
	$\Delta Ptie_1$	-0.0001082	-0.0000496	-0.0000763
	$\Delta Ptie_2$	-0.0001284	-0.0000726	-0.0000858
	$\Delta Ptie_3$	-0.0000824	-0.0000617	-0.0000524
	$\Delta Ptie_4$	-0.0000730	-0.0000504	-0.0000522
Objective Function	IAE	0.002778	0.002757	0.002809
	ISE	2.64e-6	2.055e-6	1.743e-6
	ITSE	6.009e-7	5.021e-7	5.38e-7
	ITAE	0.001091	0.001499	0.001859

E. CASE 5: INTRODUCING GRC & GDB SYSTEM NON-LINEARITIES

A more realistic scenario is examined for the effectiveness of the proposed GEO-PID controller by analyzing the effect of GDB and GRC system non-linearities. The non-linearities lead to higher deviations in frequency and tie-line power, resulting in reduced dynamic performance. In this case, SLP of 1% is applied simultaneously to all four areas. A GRC with a limit of $\pm$ 0.05 is considered. The time response of each area frequency and tie-line power deviations are shown in Fig. 15 for the non-linear model presented in Fig. 16. The transient response is compared with AC tie-line only, AC-DC parallel tie lines, and hybrid implementation of SMES to the AC-DC link. In Table 7, the effect on IAE, ISE, ITSE, ITAE, settling time, undershoot, and overshoot values is presented. The best fitness function value of ITAE is 0.008774 obtained for hybrid implementation of AC-DC tie-line and SMES. The settling time for change in frequency in all areas remains within the range of 3.859s to 5.271s. Similarly, the settling

TABLE 9. Sensitivity analysis of a four-area power system with various loading conditions, T_g, and T_t.

		Loading Conditions				T_g				T_t			
		+50%	+25%	-25%	-50%	+50%	+25%	-25%	-50%	+50%	+25%	-25%	-50%
Settling time (s)	ΔF_1	5.389	5.354	4.371	4.314	4.296	4.097	4.452	4.498	7.4	6.292	3.833	4.586
	ΔF_2	5.794	5.742	4.767	4.694	3.68	3.733	4.861	4.92	7.789	6.69	4.83	4.918
	ΔF_3	5.194	5.167	5.035	4.894	3.98	4.036	4.15	4.218	8.001	6.009	4.338	4.755
	ΔF_4	5.671	5.464	4.091	3.971	4.013	4.08	4.211	4.283	6.812	5.752	4.402	4.668
	$\Delta Ptie_1$	4.974	4.94	4.768	3.977	4.802	4.84	4.87	4.893	7.859	5.905	4.052	3.297
	$\Delta Ptie_2$	5.233	5.17	4.303	4.197	5.063	5.029	4.39	4.461	7.966	6.109	4.206	3.515
	$\Delta Ptie_3$	4.75	4.717	4.598	4.449	4.555	4.625	4.723	4.77	7.495	5.559	4.403	3.747
	$\Delta Ptie_4$	4.077	4.034	3.886	3.718	3.887	3.936	4.005	4.065	6.469	3.96	3.69	3.358
Overshoot (p.u.)	ΔF_1	-	-	-	-	-	-	-	-	0.000189	7.03e-5	-	-
	ΔF_2	-	-	-	-	-	-	-	-	0.000256	7.44e-5	-	-
	ΔF_3	-	-	-	-	-	-	-	-	9.57e-5	3.62e-5	-	-
	ΔF_4	-	-	-	-	-	-	-	-	7.91e-5	3.19e-5	-	-
	$\Delta Ptie_1$	0.0002361	0.0001967	0.0001180	7.87e-5	0.000	0.000	0.000	0.000	0.0002362	0.0001981	0.0001142	6.98e-5
	$\Delta Ptie_2$	9.87e-5	8.23e-5	4.93e-5	3.29e-5	7.97e-5	7.28e-5	5.80e-5	4.96e-5	0.0001214	7.717e-5	5.388e-5	4.04e-5
	$\Delta Ptie_3$	0.0001474	0.0001227	7.37e-5	4.91e-5	0.0001213	0.0001091	8.99e-5	8.40e-5	0.0001777	0.0001380	6.219e-5	3.84e-5
	$\Delta Ptie_4$	8.71e-6	7.21e-6	4.35e-6	2.89e-6	1.18e-5	8.03e-6	3.85e-6	2.64e-6	3.109e-5	1.76e-5	-	-
Undershoot (p.u.)	ΔF_1	-0.0047496	-0.0039580	-0.0023748	-0.0015831	-0.0035443	-0.0003366	-0.0029349	-0.0026633	-0.0036986	-0.0034508	-0.0028342	-0.0024432
	ΔF_2	-0.0045752	-0.0038127	-0.0022876	-0.0015250	-0.0033863	-0.0032270	-0.0028527	-0.0026401	-0.0035923	-0.0033402	-0.0027088	-0.0022960
	ΔF_3	-0.0050121	-0.0041767	-0.0025060	0.0016707	-0.0037033	-0.0035350	-0.0031214	-0.0028750	-0.0039129	-0.0036479	-0.0029784	-0.0025457
	ΔF_4	-0.0054122	-0.0045101	-0.0027060	-0.0018040	-0.0001023	-0.0038280	-0.0033484	-0.0030388	-0.0041959	-0.0039241	-0.0032344	-0.0027971
	$\Delta Ptie_1$	-0.0001078	-8.99e-5	-5.39e-5	-3.59e-5	-9.07e-5	-7.98e-5	-6.57e-5	-6.08e-5	-0.0001732	-0.0001195	-3.54e-5	-1.20e-5
	$\Delta Ptie_2$	-0.0001656	-0.0001380	-8.28e-5	-5.52e-5	-0.0001347	-0.0001219	-0.0001007	-9.26e-5	-0.0001882	-0.0001501	-7.17e-5	-4.09e-5
	$\Delta Ptie_3$	-0.0001062	-8.855e-5	-5.306e-5	-3.53e-5	-7.40e-5	-7.23e-5	-6.92e-5	-6.69e-5	-9.32e-5	-8.28e-5	-5.71e-5	-4.13e-5
	$\Delta Ptie_4$	-9.82e-5	-8.18e-5	-4.90e-5	3.27e-5	-7.598e-5	-7.08e-5	-6.01e-5	-5.55e-5	-8.96e-5	-7.82e-5	-5.14e-5	-3.58e-5
Objective Function	IAE	0.004126	0.003438	0.002063	0.001375	0.002752	0.002751	0.00275	0.00275	0.002909	0.002778	0.002748	0.002748
	ISE	4.86e-6	3.38e-6	1.21e-6	5.4e-6	2.51e-6	2.33e-6	2.01e-6	1.89e-6	3.07e-6	2.59e-6	1.78e-6	1.47e-6
	ITSE	1.22e-6	8.52e-7	3.07e-7	1.36e-7	5.88e-7	5.61e-7	5.39e-7	5.41e-7	7.36e-7	6.20e-7	5.09e-7	5.10e-7
	ITAE	0.001999	0.001666	0.0009997	0.0006665	0.001233	0.001282	0.001384	0.001436	0.001297	0.00119	0.001556	0.001789

TABLE 10. Sensitivity analysis of a four-area power system with variation in B, R, and T_{12}.

		B			R				T_{12}			
		+50%	+25%	-25%	+50%	+25%	-25%	-50%	+50%	+25%	-25%	-50%
Settling time (s)	ΔF_1	6.055	5.333	9.232	5.078	4.320	4.534	4.736	3.473	3.600	4.489	8.105
	ΔF_2	6.557	5.758	8.867	4.580	3.712	3.877	4.012	3.781	3.789	5.010	8.811
	ΔF_3	6.645	6.032	9.01	3.877	3.967	4.312	4.517	2.752	3.320	4.047	7.511
	ΔF_4	5.256	4.787	8.73	3.987	4.06	4.288	4.646	4.156	4.097	5.200	7.095
	$\Delta Ptie_1$	6.658	5.900	8.83	4.686	7.770	5.098	5.451	4.880	4.339	7.736	10.775
	$\Delta Ptie_2$	5.943	5.225	7.818	4.882	4.726	4.498	5.664	4.922	4.074	6.984	11.177
	$\Delta Ptie_3$	6.259	5.553	6.732	4.510	4.578	4.831	5.121	4.681	4.280	7.299	8.116
	$\Delta Ptie_4$	5.056	4.603	8.567	3.893	3.926	4.028	4.104	3.965	3.900	5.023	10.112
Overshoot (p.u.)	ΔF_1	-	-	0.0001092	-	-	-	-	-	-	-	-
	ΔF_2	-	-	0.0001746	-	-	-	-	-	-	-	-
	ΔF_3	-	-	8.45e-5	-	-	-	-	-	-	-	-
	ΔF_4	-	-	2.64e-5	-	-	-	-	-	-	-	-
	$\Delta Ptie_1$	0.0001042	0.0001263	0.0002024	0.0001604	0.00015918	0.0001545	0.00014931	0.0001573	0.0002011	0.0001140	7.18 e-5
	$\Delta Ptie_2$	4.85e-5	5.59e-5	0.0001424	6.64e-5	6.62e-5	6.52e-5	6.40e-5	6.58e-5	8.75e-5	5.10e-5	3.53e-5
	$\Delta Ptie_3$	4.99e-5	6.24e-5	3.57e-5	0.0001031	0.0001011	9.37e-5	8.55e-5	9.82e-5	0.0001483	5.99e-5	2.48e-6
	$\Delta Ptie_4$	2.08e-6	2.22e-6	0.0001752	6.56e-6	6.27e-6	5.08e-6	4.01e-6	5.81e-6	1.93e-5	3.13e-6	3.72e-5
Undershoot (p.u.)	ΔF_1	-0.0026668	-0.0028782	-0.0035741	-0.0031772	-0.0031728	-0.0031559	-0.0031265	-0.0031664	-0.0031478	-0.0031605	-0.0031625
	ΔF_2	-0.0025030	-0.0027331	-0.0035125	-0.0030616	-0.0030572	-0.0030384	-0.0030165	-0.0030499	-0.0030677	-0.0030329	-0.0030157
	ΔF_3	-0.0027873	-0.0030208	-0.0037950	-0.0033540	-0.0033489	-0.0033287	-0.0033052	-0.0033413	-0.0033418	-0.0033399	-0.0033388
	ΔF_4	-0.0030565	-0.0032901	-0.0040516	-0.0036220	-0.0036165	-0.0035940	-0.0035680	-0.0036060	-0.0035898	-0.0036135	-0.0036190
	$\Delta Ptie_1$	-3.46e-5	-4.33e-5	-0.0001846	-7.78e-5	-7.54e-5	-6.64e-5	-5.65e-5	-7.19e-5	-0.0001319	-4.49e-5	-2.89e-5
	$\Delta Ptie_2$	-5.26e-5	-7.20e-5	-0.0001785	-0.0001133	-0.0001121	-0.0001078	-0.0001034	-0.0001105	-0.0001580	-6.88e-5	-3.86e-5
	$\Delta Ptie_3$	-5.15e-5	-5.99e-5	-7.79e-5	-7.20e-5	-7.15e-5	-6.97e-5	-6.75e-5	-7.08e-5	-8.63e-5	-5.46e-5	-3.34e-5
	$\Delta Ptie_4$	-4.86e-5	-5.60e-5	-0.0001055	-6.744e-5	-6.66e-5	-6.36e-5	-6.03e-5	-6.54e-5	-8.08e-5	-4.95e-5	-3.74e-5
Objective Function	IAE	0.0027640	0.002758	0.002796	0.002754	0.002752	0.00275	0.00275	0.002751	0.002749	0.002767	0.002782
	ISE	2.63e-6	2.41e-6	1.85e-6	2.21e-6	2.19e-6	2.11e-6	2.02e-6	2.16e-6	2.16e-6	2.16e-6	2.15e-6
	ITSE	5.33e-7	5.39e-7	5.59e-7	5.60e-7	5.54e-7	5.32e-7	5.11e-7	5.45e-7	5.47e-7	5.45e-7	5.44e-7
	ITAE	0.001142	0.001217	0.001779	0.001281	0.00130	0.001392	0.001519	0.001333	0.001325	0.001413	0.001527

time for change in tie-line power remains within the range of 4.711s to 5.594s. The integration of SMES has considerably reduced frequency undershoots to 26%, 12%, 23%, and 35% for each area, respectively, without any overshoots. Moreover, $\Delta Ptie_1$ does not have any significant undershoots, however, a reduction of 4%, 38%, and 58% is observed

in $\Delta Ptie_2$, $\Delta Ptie_3$, and $\Delta Ptie_4$ undershoots, respectively. Also, the frequency oscillation settling time is improved by 11%, 5%, 10%, and 18% in each area. It is concluded that the proposed GEO-PID controller has great capability under GRC and GDC applications with the same controller gains computed in test case 2.

F. CASE6: HYBRID ENERGY STORAGE SYSTEM WITH AC-DC PARALLEL TIE-LINES

A hybrid energy storage system is investigated for the LFC in a multi-area power system. The effect of integrated VRFB and SMES is analyzed with the AC-DC parallel tie-lines in a four-area interconnected thermal power system as illustrated in Fig. 17 with the SLP of 1% applied simultaneously on all four areas. The optimized GEO-PID controller gains from case 2 are used to enhance system stability. A hybrid storage system consisting of SMES and VRFB in the presence of AC-DC tie-line is modeled and compared with AC tie-line with VRFB and AC-DC link with VRFB. From Fig. 18, the change in frequency and tie-line power for each area indicates that the hybrid implementation of VRFB and SMES offers adequate stability with fewer undershoots and overshoots when compared to VRFB with AC-DC link. ITAE's objective function value is 0.008774 and the change in frequency undershoots are reduced by 28%, 24%, 28%, and 32% for ΔF_1, ΔF_2, ΔF_3, and ΔF_4 respectively with the application of hybrid VRFB and SMES in comparison with the VRFB alone as shown in Table 8. While the overshoots in both cases are negligible. However, the settling time of the hybrid model is slightly more but it is within a range of 7.054s to 7.541s for change in frequency which is still within the acceptable range for a traditional large multiarea power system. In addition, the ITAE value is reduced by 24%. It is evident from this simulation that the proposed hybrid energy storage system with AC-DC link is beneficial for the multi-area large power system, where maintaining the under and overshoots are critical in the event of load disturbances.

The simulation shows that the proposed GEO-PID controller works seamlessly using the same controller gains as in case 2. Based on the simulation results, VRFB coupled with SMES effectively minimizes deviation peaks and fluctuations of frequency and tie-line power.

G. CASE 7: SENSITIVITY ANALYSIS

The proposed GEO-PID controller has been analyzed with varying system parameters to confirm its validity and competence. It is essential that the designed controller must be capable of handling the variations in load and uncertainty in the system as well as maintaining frequency and tie-line power fluctuations in the desired range. To demonstrate the sensitivity analysis, system parameters such as T_g, T_t, T_{12}, R, B, and loads in all areas are varied by ±50% from their nominal values for case 2. The minimum and maximum values obtained for ITAE are 0.000667 and 0.001999; settling times are within the range of 2.752s and 11.177s, overshoots are 2.08×10^{-6} p.u. and 0.000256 p.u., and undershoots are -5.41×10^{-3} p.u. and -4.17×10^{-3} p.u., respectively, for all areas as illustrated in Table 9 and Table 10. Since changing the system configuration by changing the system parameters and loading conditions, the obtained values are not reaching towards infinity which validates and confirms the robust performance of proposed GEO-PID controller is able to easily suppress the frequency oscillations in a large multi-area power system.

IV. CONCLUSION

This paper proposes a GEO-PID controller for load frequency control in a multi-area thermal power system. A Golden Eagle Optimization metaheuristic algorithm has been employed for the first time for fine-tuning of LFC controller parameters. Results indicate that the power system performance has been significantly improved with the hybrid application of VRFB and SMES, coupled with HVDC tie-lines in all areas. For a two-area power system, the GEO-PID controller with ITAE objective function significantly reduced the settling time of ΔF_1 between 45% to 70% and ΔF_2 between 26% to 52% in comparison with other optimization techniques (ALO, DA, PSO, SCA, and WOA). Similarly, in a four-area power system, the reduction in settling time for ΔF_1 is between 25% to 80%; ΔF_2 is between 13% to 79%; ΔF_3 is between 29% to 75%; and F_4 is between 18% to 70% in comparison with other optimization techniques (ALO, DA, PSO, SCA, and WOA). The superiority of the proposed controller is confirmed through the applications of GDB and GRC non-linearities where the frequency deviations stabilize within 5.271s. A sensitivity analysis has been conducted and the results found that the proposed method maintains system stability for the ±50% variation in system parameters and loading conditions. Finally, the robustness of the proposed controller is evaluated under various conditions of load disturbances. The simulation results demonstrate the effectiveness of the GEO-PID controller in dampening LFC oscillations with reduced settling time, and minimal frequency undershoots and overshoots for various loading conditions. In future work, researchers could investigate the implementation of the GEO algorithm on fractional order and hybrid cascaded controllers to improve LFC stability in large interconnected power systems. Additionally, exploring LFC stability analysis with hybrid ESS in the context of tie-line disconnection is another promising area for future research, which could make a significant contribution to the field. Pursuing these research directions would deepen the understanding of power systems and contribute to the development of more robust and efficient control strategies.

APPENDIX
SYSTEM PARAMETERS

A. TWO-AREA POWER SYSTEM

K_{p1}=120, T_{g1}=0.08s, T_{p1}=20s, T_{t1}=0.3s, R_1=2.4; K_p=112.5, T_{g2}=0.072s, T_{p2}=25s, T_{t2}=0.33s, R_2=2.7; T_{12}=0.545s, B_1=B_2=0.425.

B. FOUR-AREA POWER SYSTEM

K_{p1}=120, T_{g1}=0.08s, T_{t1}=0.3s, T_{p1}=20s, R_1=2.4 B_1= 0.425; K_{p2}=112.5, T_{g2}=0.072s, T_{t2}=0.33s, T_{p2}=25s, R_2=2.7; B_2= 0.425; K_{p3}=125, T_{g3}=0.07s, T_{t3}=0.35s, T_{p3}=20s, R_3=2.5; B_3=0.425; K_{p4}=115, Tg_4=0.085s, T_{t4}=0.375s, T_{p4}=15s, R_4=2; B_4=0.425;

Tie-line synchronizing coefficients:

T_{21}=T_{12}=T_{32}=T_{23}=T_{13}=T_{31}=T_{41}=T_{14}=0.545s.

C. HVDC, VRFB, AND SMES

HVDC: K_{DC}=1; T_{DC}=0.2s; *VRFB:* K_{RFB}=1, T_{dRFB}= 0s, T_{cRFB}=0.3s, K_{rRFB}=1; *SMES:* K_{SMES}=0.2035, T_{SMES}= 0.03s, T_1=0.2333s, T_2=0.016s, T_3=0.7087s, T_4=0.2481s.

REFERENCES

[1] D. Sharma, "Load frequency control: A literature review," *Int. J. Sci. Technol. Res.*, vol. 9, no. 2, pp. 6421–6437, 2020. Accessed: Apr. 29, 2022. [Online]. Available: http://www.ijstr.org/final-print/feb2020/Load-Frequency-Control-A-Literature-Review.pdf

[2] I. A. Khan, H. Mokhlis, N. N. Mansor, H. A. Illias, L. J. Awalin, and L. Wang, "New trends and future directions in load frequency control and flexible power system: A comprehensive review," *Alexandria Eng. J.*, vol. 71, pp. 263–308, May 2023, doi: 10.1016/j.aej.2023.03.040.

[3] P. Dey, A. Bhattacharya, and P. Das, "Tuning of power system stabilizer for small signal stability improvement of interconnected power system," *Appl. Comput. Informat.*, vol. 16, nos. 1–2, pp. 3–28, Dec. 2017, doi: 10.1016/j.aci.2017.12.004.

[4] P. Dey, S. Mitra, A. Bhattacharya, and P. Das, "Comparative study of the effects of SVC and TCSC on the small signal stability of a power system with renewables," *J. Renew. Sustain. Energy*, vol. 11, no. 3, May 2019, Art. no. 033305, doi: 10.1063/1.5085066.

[5] J. R. Nayak, B. Shaw, and B. K. Sahu, "Implementation of hybrid SSA–SA based three-degree-of-freedom fractional-order PID controller for AGC of a two-area power system integrated with small hydro plants," *IET Gener., Transmiss. Distrib.*, vol. 14, no. 13, pp. 2430–2440, Jul. 2020, doi: 10.1049/iet-gtd.2019.0113.

[6] P. Dey, A. Saha, A. Bhattacharya, and B. Marungsri, "Analysis of the effects of PSS and renewable integration to an inter-area power network to improve small signal stability," *J. Electr. Eng. Technol.*, vol. 15, no. 5, pp. 2057–2077, Sep. 2020, doi: 10.1007/s42835-020-00499-2.

[7] P. Dey, A. Saha, P. Srimannarayana, A. Bhattacharya, and B. Marungsri, "A realistic approach towards solution of load frequency control problem in interconnected power systems," *J. Electr. Eng. Technol.*, vol. 17, no. 2, pp. 759–788, Mar. 2022, doi: 10.1007/s42835-021-00913-3.

[8] H. Bevrani, H. Golpîra, A. R. Messina, N. Hatziargyriou, F. Milano, and T. Ise, "Power system frequency control: An updated review of current solutions and new challenges," *Electr. Power Syst. Res.*, vol. 194, May 2021, Art. no. 107114, doi: 10.1016/j.epsr.2021.107114.

[9] J. R. Nayak, B. Shaw, and B. K. Sahu, "Automatic generation control of small hydro plants integrated multi-area system using fuzzy based symbiotic organism search optimized hybrid PI$^{\lambda}$D fuzzy-PI$^{\lambda}$D controller," *Int. Trans. Electr. Energy Syst.*, vol. 31, no. 8, Aug. 2021, Art. no. e12954, doi: 10.1002/2050-7038.12954.

[10] P. C. Nayak, S. Mishra, R. C. Prusty, and S. Panda, "Performance analysis of hydrogen Aqua equaliser fuel-cell on AGC of wind-hydro-thermal power systems with sunflower algorithm optimised fuzzy-PDFPI controller," *Int. J. Ambient Energy*, vol. 43, no. 1, pp. 1–14, vol. 2020, 10.1080/01430750.2020.1839556.

[11] M. Sharma, S. Dhundhara, Y. Arya, and S. Prakash, "Frequency stabilization in deregulated energy system using coordinated operation of fuzzy controller and redox flow battery," *Int. J. Energy Res.*, vol. 45, no. 5, pp. 7457–7475, Apr. 2021, doi: 10.1002/er.6328.

[12] Zaheeruddin, K. Singh, and M. Amir, "Intelligent fuzzy TIDF-II controller for load frequency control in hybrid energy system," *IETE Tech. Rev.*, vol. 39, no. 6, pp. 1–17, 2021, doi: 10.1080/02564602.2021.1994476.

[13] G. Zhang, A. Daraz, I. A. Khan, A. Basit, M. I. Khan, and M. Ullah, "Driver training based optimized fractional order PI-PDF controller for frequency stabilization of diverse hybrid power system," *Fractal Fractional*, vol. 7, no. 4, p. 315, Apr. 2023, doi: 10.3390/fractalfract7040315.

[14] D. Tripathy, S. Behera, and N. B. D. Choudhury, "Implementation of Grasshopper optimization algorithm based cascaded fuzzy PD-PI controller for frequency stability in a multi-area power system," *J. Interdiscipl. Math.*, vol. 23, no. 2, pp. 335–345, Feb. 2020, doi: 10.1080/09720502.2020.1731947.

[15] P. C. Nayak, U. C. Prusty, R. C. Prusty, and S. Panda, "Imperialist competitive algorithm optimized cascade controller for load frequency control of multi-microgrid system," *Energy Sources, A, Recovery, Utilization, Environ. Effects*, pp. 1–23, Mar. 2021, doi: 10.1080/15567036.2021.1897710.

[16] P. Aryan and G. L. Raja, "Design and analysis of novel QOEO optimized parallel fuzzy FOPI-PIDN controller for restructured AGC with HVDC and PEV," *Iranian J. Sci. Technol., Trans. Electr. Eng.*, vol. 46, no. 2, pp. 565–587, Jun. 2022, doi: 10.1007/s40998-022-00484-7.

[17] A. A. A. El-Ela, R. A. El-Sehiemy, A. M. Shaheen, and A. E.-G. Diab, "Design of cascaded controller based on coyote optimizer for load frequency control in multi-area power systems with renewable sources," *Control Eng. Pract.*, vol. 121, Apr. 2022, Art. no. 105058, doi: 10.1016/j.conengprac.2021.105058.

[18] A. E. Khalil, T. A. Boghdady, M. H. Alham, and D. K. Ibrahim, "Enhancing the conventional controllers for load frequency control of isolated microgrids using proposed multi-objective formulation via artificial rabbits optimization algorithm," *IEEE Access*, vol. 11, pp. 3472–3493, Jan. 2023, doi: 10.1109/ACCESS.2023.3234043.

[19] M. A. Sobhy, H. M. Hasanien, A. Y. Abdelaziz, and M. Ezzat, "Manta ray foraging optimization algorithm-based load frequency control for hybrid modern power systems," *IET Renew. Power Gener.*, vol. 17, no. 6, pp. 1466–1487, Apr. 2023, doi: 10.1049/RPG2.12688.

[20] E. M. Ahmed, E. A. Mohamed, A. Selim, M. Aly, A. Alsadi, W. Alhosaini, H. Alnuman, and H. A. Ramadan, "Improving load frequency control performance in interconnected power systems with a new optimal high degree of freedom cascaded FOTPID-TIDF controller," *Ain Shams Eng. J.*, Feb. 2023, Art. no. 102207, doi: 10.1016/J.ASEJ.2023.102207.

[21] H. A. Behabtu, M. Messagie, T. Coosemans, M. Berecibar, K. A. Fante, A. A. Kebede, and J. Van Mierlo, "A review of energy storage technologies' application potentials in renewable energy sources grid integration," *Sustainability*, vol. 12, no. 24, pp. 1–20, Dec. 2020, doi: 10.3390/su122410511.

[22] Y. Shi, C. Eze, B. Xiong, W. He, H. Zhang, T. M. Lim, A. Ukil, and J. Zhao, "Recent development of membrane for vanadium redox flow battery applications: A review," *Appl. Energy*, vol. 238, pp. 202–224, Mar. 2019, doi: 10.1016/j.apenergy.2018.12.087.

[23] M. Sharma, S. Prakash, S. Saxena, and S. Dhundhara, "Optimal fractional-order tilted-integral-derivative controller for frequency stabilization in hybrid power system using salp swarm algorithm," *Electr. Power Compon. Syst.*, vol. 48, no. 18, pp. 1912–1931, Nov. 2020, doi: 10.1080/15325008.2021.1906792.

[24] A. Daraz, S. A. Malik, H. Mokhlis, I. U. Haq, F. Zafar, and N. N. Mansor, "Improved-fitness dependent optimizer based FOI-PD controller for automatic generation control of multi-source interconnected power system in deregulated environment," *IEEE Access*, vol. 8, pp. 197757–197775, 2020, doi: 10.1109/access.2020.3033983.

[25] C. N. S. Kalyan and G. S. Rao, "Coordinated SMES and TCSC damping controller for load frequency control of multi area power system with diverse sources," *Int. J. Electr. Eng. Informat.*, vol. 12, no. 4, pp. 747–769, Dec. 2020. [Online]. Available: https://ijeei.org/docs-10043334415fe841ffeab6d.pdf

[26] M. Heshmati, R. Noroozian, S. Jalilzadeh, and H. Shayeghi, "Optimal design of CDM controller to frequency control of a realistic power system equipped with storage devices using grasshopper optimization algorithm," *ISA Trans.*, vol. 97, pp. 202–215, Feb. 2020, doi: 10.1016/j.isatra.2019.08.028.

[27] F. Fayaz and G. L. Pahuja, "Disturbance rejection based controller for frequency control of restructured power system," *IETE J. Res.*, pp. 1–14, Jan. 2022, doi: 10.1080/03772063.2021.2021824.

[28] E. A. Mohamed, E. M. Ahmed, A. Elmelegi, M. Aly, O. Elbaksawi, and A.-A. A. Mohamed, "An optimized hybrid fractional order controller for frequency regulation in multi-area power systems," *IEEE Access*, vol. 8, pp. 213899–213915, 2020, doi: 10.1109/access.2020.3040620.

[29] E. Çelik, N. Öztürk, Y. Arya, and C. Ocak, "(1 + PD)-PID cascade controller design for performance betterment of load frequency control in diverse electric power systems," *Neural Comput. Appl.*, vol. 33, no. 22, pp. 15433–15456, Nov. 2021, doi: 10.1007/s00521-021-06168-3.

[30] H. H. Ali, A. M. Kassem, M. Al-Dhaifallah, and A. Fathy, "Multi-verse optimizer for model predictive load frequency control of hybrid multi-interconnected plants comprising renewable energy," *IEEE Access*, vol. 8, pp. 114623–114642, 2020, doi: 10.1109/access.2020.3004299.
[31] M. K. Das, P. Bera, and P. P. Sarkar, "PID-RLNN controllers for discrete mode LFC of a three-area hydrothermal hybrid distributed generation deregulated power system," *Int. Trans. Electr. Energy Syst.*, vol. 31, no. 5, May 2021, doi: 10.1002/2050-7038.12837.
[32] A. Prakash, K. Kumar, and S. K. Parida, "PIDF(1+FOD) controller for load frequency control with SSSC and AC–DC tie-line in deregulated environment," *IET Gener., Transmiss. Distrib.*, vol. 14, no. 14, pp. 2751–2762, Jul. 2020, doi: 10.1049/iet-gtd.2019.1418.
[33] Clarivate. (2022). *Web of Science*. [Online]. Available: https://www.scopus.com/
[34] A. Kumar and M. N. Anwar, "Parallel control structure scheme for load frequency controller design using direct synthesis approach," *Int. J. Electr. Comput. Eng.*, vol. 10, no. 1, pp. 47–60, Feb. 2020, doi: 10.11591/IJECE.V10I1.PP47-60.
[35] W. Tan, "Decentralized load frequency controller analysis and tuning for multi-area power systems," *Energy Convers. Manage.*, vol. 52, no. 5, pp. 2015–2023, May 2011, doi: 10.1016/J.ENCONMAN.2010.12.011.
[36] E. Ozkop, I. Altas, and A. M. Sharaf, "Load frequency control in four area power systems using fuzzy logic PI controller," in *Proc. 16th Nat. Power Syst. Conf.*, Dec. 2010, pp. 233–240. Accessed: Nov. 10, 2022. [Online]. Available: https://www.researchgate.net/publication/259570489_Load_Frequency_Control_in_Four_Area_Power_Systems_Using_Fuzzy_Logic_PI_Controller
[37] P. J. Krishna, V. P. Meena, and V. P. Singh, "Load frequency control in four-area interconnected power system using fuzzy PI controller with penetration of renewable energies," in *Proc. 2nd Int. Conf. Power, Control Comput. Technol. (ICPCT)*, Mar. 2022, pp. 1–6, doi: 10.1109/ICPC2T53885.2022.9777076.
[38] E. Sahin, "Design of an optimized fractional high order differential feedback controller for load frequency control of a multi-area multi-source power system with nonlinearity," *IEEE Access*, vol. 8, pp. 12327–12342, 2020, doi: 10.1109/access.2020.2966261.
[39] R. K. Sahu, T. S. Gorripotu, and S. Panda, "Automatic generation control of multi-area power systems with diverse energy sources using teaching learning based optimization algorithm," *Eng. Sci. Technol., Int. J.*, vol. 19, no. 1, pp. 113–134, Mar. 2016, doi: 10.1016/J.JESTCH.2015.07.011.
[40] A. Daraz, S. Abdullah, H. Mokhlis, I. U. Haq, G. Fareed, and N. N. Mansor, "Fitness dependent optimizer-based automatic generation control of multi-source interconnected power system with non-linearities," *IEEE Access*, vol. 8, pp. 100989–101003, 2020, doi: 10.1109/access.2020.2998127.
[41] P. Bhui, N. Senroy, A. K. Singh, and B. C. Pal, "Estimation of inherent governor dead-band and regulation using unscented Kalman filter," *IEEE Trans. Power Syst.*, vol. 33, no. 4, pp. 3546–3558, Jul. 2018, doi: 10.1109/TPWRS.2017.2765692.
[42] W. Tan, S. Chang, and R. Zhou, "Load frequency control of power systems with non-linearities," *IET Gener., Transmiss. Distrib.*, vol. 11, no. 17, pp. 4307–4313, Nov. 2017, doi: 10.1049/iet-gtd.2017.0599.
[43] S. Priyadarshani, K. R. Subhashini, and J. K. Satapathy, "Pathfinder algorithm optimized fractional order tilt-integral-derivative (FOTID) controller for automatic generation control of multi-source power system," *Microsyst. Technol.*, vol. 27, no. 1, pp. 23–35, Jan. 2021, doi: 10.1007/S00542-020-04897-4.
[44] H. Gozde and M. C. Taplamacioglu, "Automatic generation control application with craziness based particle swarm optimization in a thermal power system," *Int. J. Electr. Power Energy Syst.*, vol. 33, no. 1, pp. 8–16, Jan. 2011, doi: 10.1016/j.ijepes.2010.08.010.
[45] M. Sharma, S. Prakash, and S. Saxena, "Robust load frequency control using fractional-order TID-PD approach via salp swarm algorithm," *IETE J. Res.*, pp. 1–17, Apr. 2021, doi: 10.1080/03772063.2021.1905084.
[46] A. Mohammadi-Balani, M. D. Nayeri, A. Azar, and M. Taghizadeh-Yazdi, "Golden eagle optimizer: A nature-inspired metaheuristic algorithm," *Comput. Ind. Eng.*, vol. 152, pp. 1–45, Feb. 2021, doi: 10.1016/j.cie.2020.107050.
[47] N. Chuang, "Robust H_∞ load-frequency control in interconnected power systems," *IET Control Theory Appl.*, vol. 10, no. 1, pp. 67–75, Jan. 2016, doi: 10.1049/IET-CTA.2015.0412.
[48] Y. V. Hote and S. Jain, "PID controller design for load frequency control: Past, present and future challenges," *IFAC-PapersOnLine*, vol. 51, no. 4, pp. 604–609, Jan. 2018, doi: 10.1016/J.IFACOL.2018.06.162.
[49] W. Tan and H. Zhou, "Robust analysis of decentralized load frequency control for multi-area power systems," *Int. J. Electr. Power Energy Syst.*, vol. 43, no. 1, pp. 996–1005, Dec. 2012, doi: 10.1016/j.ijepes.2012.05.063.
[50] A. Daraz, S. A. Malik, I. U. Haq, K. B. Khan, G. F. Laghari, and F. Zafar, "Modified PID controller for automatic generation control of multi-source interconnected power system using fitness dependent optimizer algorithm," *PLoS ONE*, vol. 15, no. 11, Nov. 2020, Art. no. e0242428, doi: 10.1371/journal.pone.0242428.
[51] D. Mishra, P. C. Nayak, S. K. Bhoi, and R. C. Prusty, "Design and analysis of multi-stage TDF/(1+TI) controller for load-frequency control of A.C multi-islanded microgrid system using modified sine cosine algorithm," in *Proc. 1st Odisha Int. Conf. Electr. Power Eng., Commun. Comput. Technol. (ODICON)*, Jan. 2021, pp. 1–6, doi: 10.1109/ODICON50556.2021.9428969.
[52] A. H. Gomaa Haroun and Y.-Y. Li, "Ant lion optimized fractional order fuzzy pre-compensated intelligent pid controller for frequency stabilization of interconnected multi-area power systems," *Appl. Syst. Innov.*, vol. 2, no. 2, p. 17, May 2019, doi: 10.3390/asi2020017.

IRFAN AHMED KHAN received the B.S. degree in electronics from the Sir Syed University of Engineering and Technology, Pakistan, in 2007, and the M.S. degree in electrical engineering from the King Fahd University of Petroleum and Minerals, Saudi Arabia, in 2012. He is currently pursuing the Ph.D. degree in electrical engineering with Universiti Malaya, Malaysia. His research interests include load frequency control, power system modeling and optimization, control systems, hybrid energy storage systems, wide area measurements, FACTS, and renewable energy.

HAZLIE MOKHLIS (Senior Member, IEEE) received the B.Eng. and M.Eng.Sc. degrees in electrical engineering from Universiti Malaya (UM), Malaysia, in 1999 and 2002, respectively, and the Ph.D. degree from The University of Manchester, Manchester, U.K., in 2009. He is currently a Professor with the Department of Electrical Engineering, UM, and the Head of the UM Power and Energy System (UMPES) Research Group. He is also a Chartered Engineer in U.K. and a Professional Engineer in Malaysia. His research interests include fault location, distribution automation, power system protection, and renewable energy.

NURULAFIQAH NADZIRAH MANSOR (Senior Member, IEEE) received the B.Eng. degree from Vanderbilt University, USA, in 2008, the M.Eng. degree in power system engineering from Universiti Malaya, Malaysia, in 2013, and the Ph.D. degree from The University of Manchester, U.K., in 2018. From 2008 to 2014, she was a Process Engineer with Texas Instruments (M). She is currently a Senior Lecturer with Universiti Malaya. Her research interests include distribution system modeling and optimization, distribution system planning and operation, the integration of renewable energy, and smart grids.

HAZLEE AZIL ILLIAS (Senior Member, IEEE) received the B.Eng. degree from Universiti Malaya, Malaysia, in 2006, and the Ph.D. degree in electrical engineering from the University of Southampton, U.K., in 2011. He is currently an Associate Professor with the Department of Electrical Engineering, Universiti Malaya, and the Head of the Universiti Malaya High Voltage Research Group. His research interests include PD modeling and measurement, condition monitoring, lightning overvoltage, and artificial intelligent application in high-voltage engineering.

MUHAMMAD USAMA received the B.Sc. degree in electrical engineering from the University of Central Punjab, Lahore, Pakistan, in 2012, the M.Sc. degree in electrical engineering from the University of Engineering and Technology (UET) Lahore, in 2017, and the Ph.D. degree in the protection of smart distribution networks from Universiti Malaya (UM). His current research interests include power system analysis and stability, smart distribution networks, and power system protection.

AMIL DARAZ was born in Pakistan, in 1989. He received the B.E. degree in electronics engineering from COMSATS University Islamabad, Pakistan, in 2012, and the M.S. degree in power and control engineering and the Ph.D. degree in electrical engineering from International Islamic University Islamabad (IIUI), Pakistan. He is currently a Postdoctoral Researcher with NingboTech University, Ningbo, China. His research interests include control systems, power system operation and control, and the optimization of solving nonlinear problems.

LI WANG (Senior Member, IEEE) received the Ph.D. degree in electrical engineering from the National Taiwan University, Taipei, Taiwan, in June 1988. He was an Associate Professor with the Department of Electrical Engineering, National Cheng Kung University, Tainan, Taiwan, from 1988 to 1995. He has been a Professor with the Department of Electrical Engineering, National Cheng Kung University, Tainan, since 1995. He was a Visiting Scholar with the School of Electrical Engineering and Computer Science, Purdue University, West Lafayette, IN, USA, from February to July 2000. He was a Visiting Scholar with the School of Electrical Engineering and Computer Science, Washington State University, Pullman, WA, USA, from August 2003 to January 2004. He was a Research Scholar with the Energy Systems Research Center, The University of Texas at Arlington, TX, USA, from July 2008 to January 2009. He is currently with the Department of Electrical Engineering, National Cheng Kung University. His research interests include power systems stability and renewable energy.

LILIK JAMILATUL AWALIN was born in East Java, Indonesia, in 1977. She received the B.Eng. degree in electrical engineering from the University of Widya Gama, in 1999, the M.Eng. degree from Institut Teknologi Sepuluh Nopember, Indonesia, in 2004, and the Ph.D. degree from Universiti Malaya in 2014. She was a Senior Lecturer with the Electrical Engineering Section, British Malaysia Institute, University Kuala Lumpur, Malaysia, from 2015 to 2020. Currently, she is a Senior Lecturer with Airlangga University, Indonesia. Her research interests include fault locations, protection systems, distribution and transmission systems, and smart grids.